Chem

CellPress

Article

Capturing the Quenching Mechanism of Light-Harvesting Complexes of Plants by Zooming in on the Ensemble

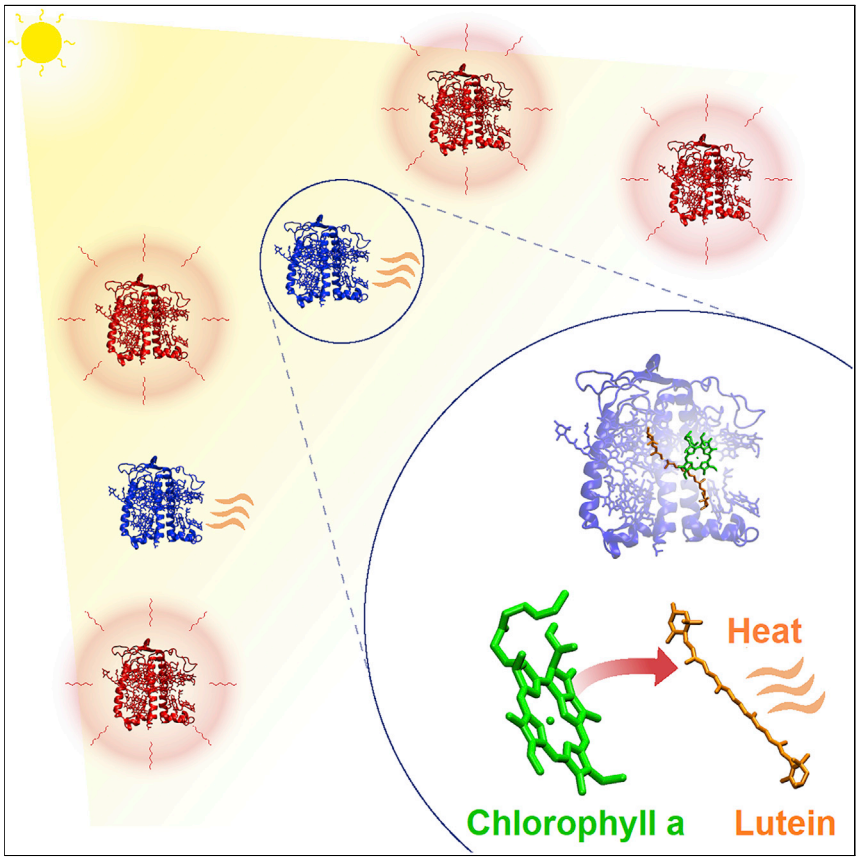

To cope with changing light conditions, the light-harvesting complexes of plants can switch between a highly fluorescent state, where they can act as antennae, and a quenched state, where the excess absorbed energy is safely dissipated as heat to avoid photodamage. This study reveals that in CP29, a minor antenna of plants, energy transfer from specific chlorophylls to a debated carotenoid excited state is responsible for the photoprotective mechanism.

Vincenzo Mascoli, Nicoletta Liguori, Pengqi Xu, Laura M. Roy, Ivo H.M. van Stokkum, Roberta Croce

r.croce@vu.nl

HIGHLIGHTS

Uncovered the photoprotective mechanism of light-harvesting complexes of plants

Observed a carotenoid dark state that quenches chlorophyll excitations

Located the quenching site inside the complex

Mascoli et al., Chem 5, 1–13
November 14, 2019
https://doi.org/10.1016/j.chempr.2019.08.002

Please cite this article in press as: Mascoli et al., Capturing the Quenching Mechanism of Light-Harvesting Complexes of Plants by Zooming in on the Ensemble, Chem (2019), https://doi.org/10.1016/j.chempr.2019.08.002

Chem

CellPress

Article

Capturing the Quenching Mechanism of Light-Harvesting Complexes of Plants by Zooming in on the Ensemble

Vincenzo Mascoli,[1] Nicoletta Liguori,[1] Pengqi Xu,[1] Laura M. Roy,[1] Ivo H.M. van Stokkum,[1] and Roberta Croce[1,2,*]

SUMMARY

The light-harvesting complexes (LHCs) of plants can regulate the energy flux to the reaction centers in response to fluctuating light by virtue of their vast conformational landscape. They do so by switching from a light-harvesting state to a quenched state, dissipating the excess absorbed energy as heat. However, isolated LHCs are prevalently in their light-harvesting state, which makes the identification of their photoprotective mechanism extremely challenging. Here, ensemble time-resolved fluorescence experiments show that monomeric CP29, a minor LHC of plants, exists in various emissive states with identical spectra but different lifetimes. The photoprotective mechanism active in a subpopulation of strongly quenched complexes is further investigated via ultrafast transient absorption spectroscopy, kinetic modeling, and mutational analysis. We demonstrate that the observed quenching is due to excitation energy transfer from chlorophylls to a dark state of the centrally bound lutein.

INTRODUCTION

In plants and green algae, photosynthetic reactions start with light absorption by pigment-protein complexes embedded in the thylakoid membrane. Such antenna proteins efficiently deliver the absorbed energy to the reaction centers, where it is used to promote charge separation, the initial step of converting light to energy. Effective regulation of this energy flux in response to changing light conditions is necessary for plants to avoid photodamage and optimize growth.[1,2] Antenna proteins play a crucial role in these regulatory mechanisms, being able to switch conformation and, consequently, their functional state: from highly fluorescent states, whose long excited-state lifetime is imperative for light harvesting, to short lifetime (quenched) states, carrying out photoprotection by safely dissipating excitation energy as heat.[3–7]

But what is the quenching mechanism? Although many studies have addressed this question, the answer is still debated because of the technical challenges of the measurements. In principle, the most suitable way to study the mechanism of quenching would be to perform time-resolved spectroscopic measurements on isolated monomeric light-harvesting complexes (LHC). This permits the control of the experimental conditions, and the relatively low number of pigments per protein helps to avoid power-dependent artifacts such as annihilation.[8,9] Moreover, the above-mentioned conformational variety has been disclosed by single-molecule techniques for a wide range of isolated LHCs.[10,11] However, such a variegated landscape usually falls through the net of bulk experiments due to ensemble

The Bigger Picture

The light-harvesting complexes of plants have a dual and seemingly opposite role: in low light they act as antennae, collecting energy for photochemistry, whereas in high light they switch to a quenched state, dissipating the excess absorbed energy as heat to avoid photodamage. Quenching is necessary for plants to survive in high light but also causes a drop in photosynthetic efficiency. Unveiling the photoprotective mechanism is therefore important for improving crop productivity. The identification of the quenching mechanism is hindered by the fact that, in isolated solubilized complexes, the light-harvesting conformation largely dominates. Here, we have taken advantage of the presence of a subpopulation of quenched complexes in the ensemble of isolated proteins to simultaneously analyze the light-harvesting and quenched states. This allowed us to understand the nature of the photoprotective mechanism and to identify the quenching site.

Please cite this article in press as: Mascoli et al., Capturing the Quenching Mechanism of Light-Harvesting Complexes of Plants by Zooming in on the Ensemble, Chem (2019), https://doi.org/10.1016/j.chempr.2019.08.002

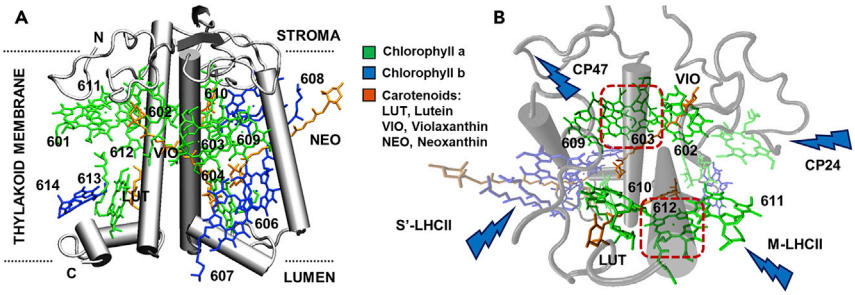

Figure 1. CP29 Structure

Side view of CP29 structure (A)[25] and stromal view of CP29 (B). The clusters of chlorophylls forming the terminal emitter domains are highlighted, together with the centrally bound carotenoids and the energy transfer connections with surrounding complexes in photosystem II[25] (the blue lightning bolts indicate the direction of energy transfer). The long N-terminal loop is left out for clarity.

averaging. When isolated, the vast majority of LHCs are found in a highly fluorescent light-harvesting state, and ensemble measurements generally fail to capture any detailed information about the quenched state.[7,12,13] Promoting the photoprotective state of photosynthetic complexes *in vitro* is possible but requires protein aggregation,[14,15] crystallization,[3] or embedding into gel matrices in the absence of detergent.[16] These conditions, however, pose more experimental challenges[9,17] and might be more difficult to relate to physiological conditions. As a result, the investigation of antenna quenching *in vitro* remains a complicated task, and the exact nature of the photoprotective mechanism is still controversial.[17–20]

Only two cases have been reported so far of solubilized monomeric antennae that are constitutively in a quenched state.[21,22] Both studies evidenced the involvement of a carotenoid excited state as a quencher of chlorophyll excitation. Staleva et al.[21] showed that a carotenoid S_1 state could efficiently quench chlorophyll in one of the cyanobacterial light-inducible proteins (Hlips), which are generally regarded as the ancestors of modern LHCs.[23] More recently, our group demonstrated that in a LHC from a mutant tobacco plant containing astaxanthin, chlorophyll excitation is constitutively quenched by the astaxanthin S* state, which becomes accessible via a twist of the carotenoid end-ring.[22] However, the experimental proof that the same quenching mechanism is active in LHCs with their natural pigment content is still missing.

In this work, we were able to identify different emissive states in a wildtype monomeric LHC from plants in a bulk experiment. The antenna investigated is CP29, one of the minor LHCs of plants and algae, which is part of the photosystem II supercomplex.[24,25] It is an integral membrane protein binding 13–14 chlorophylls (mostly chlorophylls a) and 3 carotenoids (Figure 1A).[25–27] CP29 occupies a central position in the energy transfer routes of photosystem II, receiving excitations from peripheral LHCII and delivering them to the core protein CP47 (Figure 1B), and it was also shown to play a role in photoprotection.[28,29] All our measurements were performed on the solubilized monomeric protein. Most of the complexes were in their unquenched light-harvesting state, but a significant subset was found in a strongly quenched state.

The nature of the observed photoprotective mechanism and of the pigments involved was investigated by a combination of time-resolved spectroscopy, compartmental target modeling, and mutational analysis.

[1]Department of Physics and Astronomy and Institute for Lasers, Life and Biophotonics, Faculty of Sciences, Vrije Universiteit Amsterdam, De Boelelaan 1081, 1081 HV Amsterdam, the Netherlands

[2]Lead Contact

*Correspondence: r.croce@vu.nl

https://doi.org/10.1016/j.chempr.2019.08.002

Please cite this article in press as: Mascoli et al., Capturing the Quenching Mechanism of Light-Harvesting Complexes of Plants by Zooming in on the Ensemble, Chem (2019), https://doi.org/10.1016/j.chempr.2019.08.002

Table 1. Lifetime Components and Relative Amplitudes for 680 nm Emission (468 Excitation) of CP29 WT and Mutants at 10°C

	τ_1 (ns)	%	τ_2 (ns)	%	τ_3 (ns)	%	τ_{avg} (ns)
CP29 WT	0.09	16	1.56	14	4.06	70	3.08
KO 612	0.20	9	2.03	19	4.26	72	3.47
KO 603	0.09	14	1.58	11	4.27	75	3.39

Each fraction has an uncertainty $\leq \pm 1\%$ (estimated by simultaneously analyzing three different replicas of each sample). Parameter 95% confidence intervals are $\leq \pm 0.03$ ns for τ_1, $\leq \pm 0.15$ ns for τ_2, $\leq \pm$ 0.03 ns for τ_3, and $\leq \pm 1\%$ on all fractional amplitudes (see Figures S1 and S14 for the fluorescence decay traces).

RESULTS

Time-Resolved Fluorescence and Transient Absorption Reveal Lifetime Heterogeneity

Time-resolved fluorescence traces of CP29 measured at room temperature at 680 nm upon 468 nm excitation required three lifetime components for proper fitting (first row of Table 1; Figure S1). The larger contribution (70%) stems from a 4.1 ns component. The remaining contributions are from a 1.6 ns (about 14% of total signal) and a ~100 ps (16% of total amplitude) component. The resulting average lifetime is around 3.1 ns.

Time-resolved fluorescence traces obtained after 468 nm excitation were measured at different emission wavelengths (Figure S2) and globally analyzed to obtain the decay-associated spectrum (DAS) of each component (Figure 2A). The average lifetime is essentially wavelength independent, and all the three DAS have a profile identical to that of the steady-state spectrum of the complex (Figures 2 and S3).

The lifetime heterogeneity, which is observed in many antenna proteins,[12,13,30,31] can be explained by the presence of different emissive states of CP29, with the majority of the complexes exhibiting a long lifetime (about 4 ns). A smaller but significant fraction of antennae is found in slightly (1.6 ns) and strongly (~0.1 ns) quenched states. The high similarity of the fluorescence spectra of these states implies that the terminal emitter domain of all is identical. This suggests that red-emitting (e.g., chlorophyll-chlorophyll charge transfer[32,33]) states do not play a role in the quenching mechanism and supports the idea that the quencher in CP29 is a dark (non-emissive) state populated from chlorophyll excited states. It should be noted that previous studies have shown that the lifetime heterogeneity observed here in CP29 is an intrinsic property of all LHCs not only in detergent[11,12,31,34–36] but also in liposomes,[12,37,38] lipid nanodisks,[39] and the thylakoid membrane,[6,40] suggesting that the conformations observed here are the same occurring *in vivo*.

To shed light on the quenching mechanism, we performed transient absorption (TA) measurements on CP29 in its monomeric state. This technique allows the observation of dark states (such as carotenoid excited states), which cannot be detected with fluorescence measurements.[41] The monomers were excited in the red edge of the absorption spectrum (682 nm; see Figure S4) and a large part of the visible was probed (from 480 to 720 nm) to be able to identify carotenoid excited states possibly involved in quenching. Two additional experiments were performed with 489 and 509 nm excitation wavelengths (direct carotenoid excitation) in order to extract the spectra of the carotenoid excited states. Global analysis was performed on all measured data (Figures 3A and 3B; see Experimental Procedures

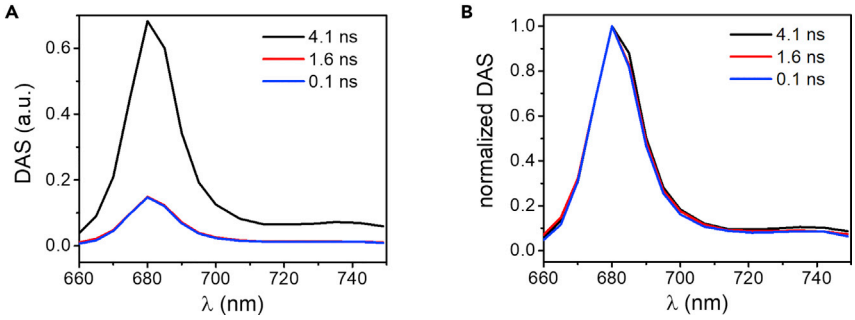

Figure 2. Time-Resolved Fluorescence Experiments

DAS (A) and normalized DAS (B) for time-resolved emission of CP29 WT upon 468 nm excitation (see also Figures S2 and S15).

for details on data analysis). In first approximation, a sequential scheme can be used to describe the data (Figure 3C), with each species (evolution-associated difference spectrum [EADS]; Figure 3E) decaying into the following one with a specific lifetime. Since the resolved lifetimes are well separated, the resulting DADS (decay-associated difference spectra, which originate instead from a parallel kinetic scheme; Figures 3D, 3F, and S5) are essentially the spectral difference between consecutive EADS.

After excitation in the Qy band, the signal is dominated by a bleach in the Qy region due to ground-state bleaching and stimulated emission of chlorophyll excited states (blue signal in Figure 3B; black, red, and blue EADS in Figure 3E). A small positive signal at wavelengths < 600 nm is due to chlorophyll excited-state absorption (ESA; the weak red signal in Figures 3A and 3B). Global analysis of the TA data for the 682 nm excitation reveals four main components (see EADS in Figure 3E and DADS in Figure S5). Energy equilibration between different pools of chlorophylls (mostly involving uphill energy transfer; see black to red EADS in Figure 3E and blue DADS in Figure S5) takes place in 2.4 ps, in agreement with previous reports,[42,43] followed by a loss of 16% of the total bleach in 54 ps (red to blue EADS). The remaining bleach (blue EADS) decays in 2.4 ns, populating a long-lived species (green EADS), whose lifetime is far longer than the experimental time window. Such a component can be assigned to a mix of carotenoid and chlorophyll triplet states.[44] The fractions and lifetimes of the 54 ps and of the 2.4 ns components (represented by the DADS of Figure 3F) are consistent with what was observed in time-resolved fluorescence measurements (with the difference that the two long-lifetime components of 1.6 and 4 ns are merged into one single nanosecond component due to the limited experimental time window). The lifetime of 54 ps for the quenched component is also a more precise estimate as compared to the lifetime obtained via TCSPC owing to the higher time resolution of TA (100 fs versus 100 ps). We can therefore relate the fast component (red DADS in Figure 3F) to the fraction of strongly quenched monomers and the slow component (blue DADS in Figure 3F) to the unquenched complexes. Notably, the quenched and unquenched components have very similar shapes and both peak at 681 nm (inset of Figure 3F). The excellent overlap in the emissive region is consistent with our time-resolved fluorescence data (Figure 2B) and shows that the quenching in CP29 is not related to red-emitting states. Compared to the chlorophyll ESA profile shown by EADS 1, 2, and 3 in Figures 3C–3E, the DADS of the 54 ps component displays larger amplitude at shorter wavelengths, suggesting the involvement of a quencher which does not have a chlorophyll excited-state character (and whose spectrum peaks instead in the 500–520 nm region; see Figure S5).

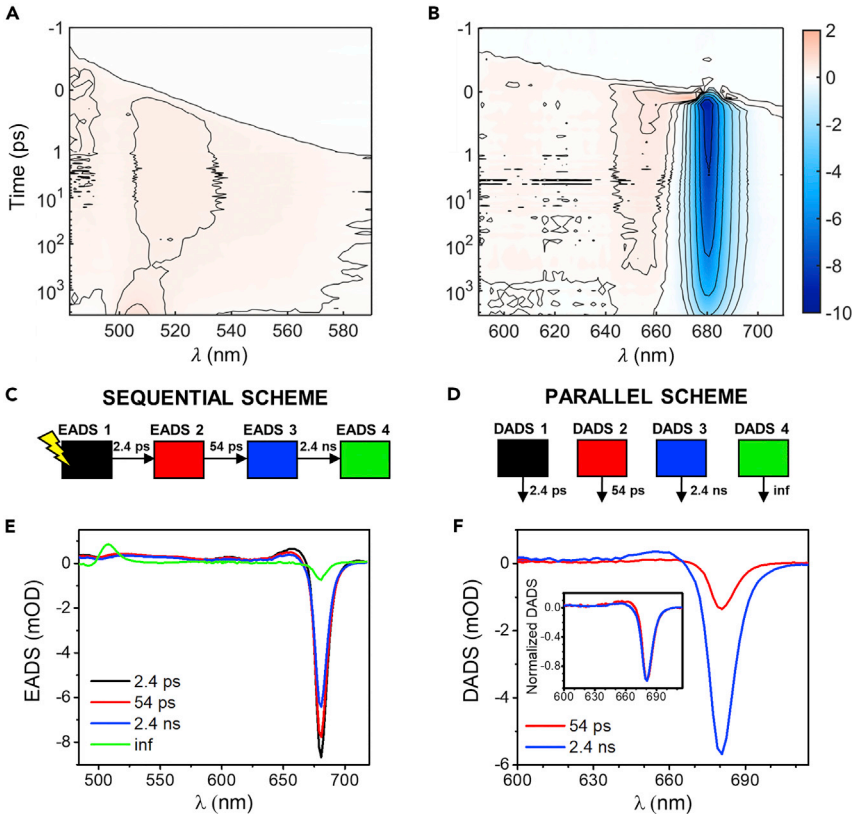

Figure 3. Transient Absorption Experiments

2D representation of measured TA data of CP29 WT excited at 682 nm and probed in the high-energy (480–590 nm; A) and low-energy (Qy, 590–710 nm; B) regions. The time scale is linear between −1 and 1 ps and logarithmic thereafter (see also Figure S7 for the time traces). Sequential (C) and parallel (D) schemes for global analysis resulted in EADS (E) and DADS (F), respectively. (F) only shows DADS for quenched (red) and unquenched (blue) components. See Figure S5 for the complete set of DADS. Inset of (F) shows normalized DADS for quenched and unquenched components.

Heterogeneous Target Modeling Highlights the Involvement of a Carotenoid Dark State in the Quenching

We have so far demonstrated that detergent-solubilized CP29 exhibits a heterogeneous distribution of lifetimes, ranging from 4 ns to less than 100 ps. Both time-resolved fluorescence and TA data exclude the contribution of chlorophyll-chlorophyll charge-transfer states in the spectra of the quenched complexes, indicating that the terminal emitter domain in both quenched and unquenched CP29 is a purely excitonic state. In light of this finding, the strong lifetime reduction in quenched complexes implies the existence of a short-lived dark state able to quench chlorophyll excitations. To resolve the spectra of the pigments active in energy transfer, we therefore applied a compartment target model to the 682 nm excitation dataset. Each compartment represents a species with a difference spectrum (SADS [species-associated difference spectrum]).[45] Compartments can communicate via energy transfer processes whose rates (and connectivity) are determined to reproduce the measured kinetics (Figure 4A). To account for the heterogeneity of CP29 emission lifetimes, the model adopts two parallel schemes referring to unquenched and quenched complexes (Figure 4A), each containing three compartments. In the scheme representing unquenched complexes (violet box), energy equilibration between two pools of chlorophylls (red and cyan compartments) is followed by the

Please cite this article in press as: Mascoli et al., Capturing the Quenching Mechanism of Light-Harvesting Complexes of Plants by Zooming in on the Ensemble, Chem (2019), https://doi.org/10.1016/j.chempr.2019.08.002

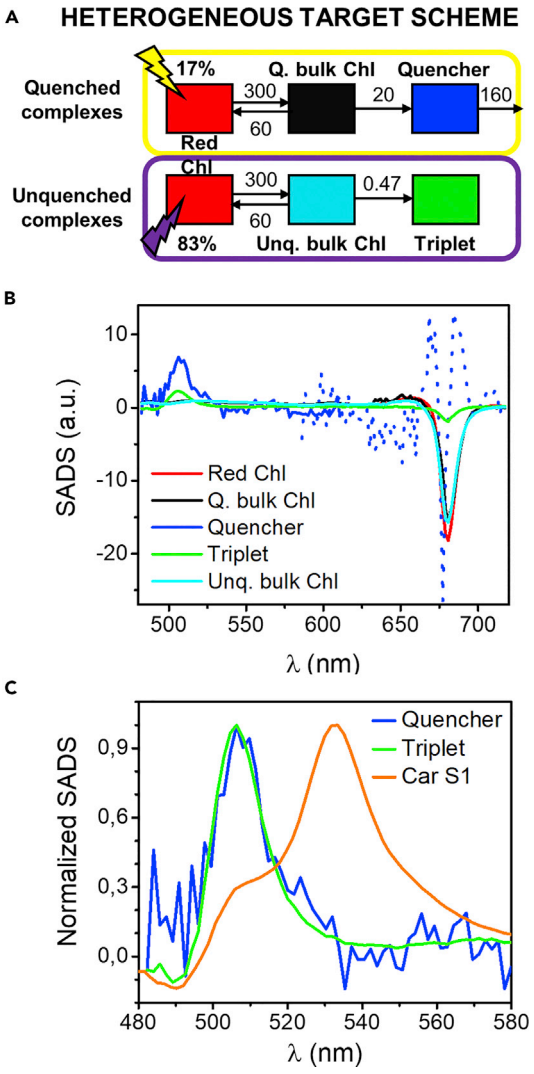

Figure 4. Heterogeneous Target Modeling Highlights the Involvement of a Carotenoid Dark State in the Quenching

(A) Heterogeneous model for target analysis of 682 nm excitation data. The six compartments, each represented by a colored rectangle, are grouped into quenched (yellow box) and unquenched (violet box) complexes. The amount of initial excitation, related to the fraction of quenched/unquenched monomers in the ensemble, is represented by the lightning bolts. The compartments are connected by arrows representing energy transfer processes, whose rates are given in ns^{-1} (see also Figures S6, S10, and S13 and Text S1).

(B) Species-associated difference spectra (SADS) of each compartment in the target model. The quencher spectrum in the Qy region is dotted to allow better visualization of the chlorophyll SADS (see also Figures S6, S10, and S13 and Texts S1 and S2).

(C) Overlay of the normalized SADS of the quencher (blue), carotenoid triplet (green), and carotenoid S_1 (orange) from TA data on CP29 (see Figures S11 and S12 and Text S1 for details).

decay of their excited state in a few nanoseconds, which populates long-lived triplets (triplet formation is approximated as a one-step process from the cyan to the green compartment). In the scheme of the quenched complexes (yellow box), an identical energy equilibration between chlorophylls (red and black compartments) precedes energy transfer with a rate of 20/ns to a quencher (blue compartment). The quencher finally decays with a rate of 160/ns. Because of these inverted kinetics, the concentration of the quencher will remain small (see Figure S6). At time zero, only the red chlorophyll pools are excited, and the amount of excitation going into the quenched and unquenched compartment groups represents the fraction of quenched/unquenched complexes. More details about the compartmental model are given in Text S1.

Because of the weaker signal at wavelengths below 630 nm, the fitting in this region is very sensitive and required additional constraints on the shape of the ESA of different chlorophyll compartments. We therefore tested different sets of equality constraints (see Text S1 and Figures S7–S10 for details); the obtained quencher SADS, despite some spectral changes, always exhibited typical features of carotenoid excited states. The model leading to the best fitting is discussed below.

Please cite this article in press as: Mascoli et al., Capturing the Quenching Mechanism of Light-Harvesting Complexes of Plants by Zooming in on the Ensemble, Chem (2019), https://doi.org/10.1016/j.chempr.2019.08.002

The first two compartments (red and black-cyan) in both quenched and unquenched complexes represent chlorophyll pools that equilibrate in a few picoseconds. The spectral bleach of bulk unquenched chlorophylls (cyan SADS in Figure 4B) has more amplitude in the region between 660 and 675 nm than that of the red chlorophyll pool (red SADS in Figure 4B), compatible with an uphill energy equilibration taking place after selective excitation at 682 nm. The triplet spectrum (green SADS; Figure 4B) has a peak around 505 nm and a shallow bleach below 500 nm, which is typical for lutein triplets in LHCs.[44]

Note that by equating in the model the minima of the Qy bleach for unquenched and quenched bulk chlorophylls (implying that the two emissive states have similar oscillator strength), we obtained that the amount of initial excitation sitting on quenched (unquenched) complexes is 17% (83%) of the total (Figure 4A), meaning that the number of quenched monomers is around 1/6 of the total. This agrees with the fraction of strongly quenched complexes estimated from time-resolved fluorescence traces at 680 nm (16%; see Table 1).

The shape of the quencher spectrum (blue SADS in Figures 4B and 4C) does not have the characteristics of a xanthophyll S_1 state, since it peaks at shorter wavelengths than expected.[46,47] This can be appreciated by comparing the quencher spectrum to the S_1 spectrum obtained upon direct carotenoid excitation (see Figure S11 for details), which has a maximum at 532 nm and decays in around 13 ps (orange SADS in Figure 4C). Strikingly, the spectrum of the quencher resembles that of the carotenoid triplet (green SADS in Figure 4C), but it has the lifetime (around 6 ps) of a singlet carotenoid excited state[48] (carotenoid triplets have instead lifetimes of several microseconds). Based on these characteristics, we assign the quencher species to a carotenoid S* state,[49–52] since similar properties for carotenoid S* states have been observed for many other carotenoids in solution[47,51,53,54] and in LHCs[22,49,50] (as an example, Figure S12 shows a comparison between the S_1, S*, and triplet spectra of the carotenoid spheroidene as obtained in the work of Papagiannakis et al.[49] from TA experiments on the LH2 antenna of *Rb. Sphaeroides*). The quencher spectrum also shows a wavy signal in the Qy region (dotted blue line in Figure 4B), consistent with what was previously observed.[22,55] However, because of the very low concentration of the quencher (see Figure S6 for concentration profiles of all species) and the high absolute intensity of the Qy bleach, the contribution of this feature to the dynamics in the Qy region is practically negligible (see Text S2 for further discussion).

To further confirm the involvement of a carotenoid excited state in CP29 quenching, an alternative heterogeneous scheme without the quencher compartment, implying that quenched chlorophyll quickly decays without any additional quencher (see Figure S13A), was tested. Despite yielding a similar fitting quality, such a model results in an unusual ESA profile for the quenched chlorophyll compartment (Figure S13B). This SADS, which is markedly different from that of all other chlorophyll species (Figure S13C), exhibits a peak in the carotenoid triplet region (i.e., where the quencher SADS would peak according to the above discussed heterogeneous model; compare Figures S13 and 4). Such an unrealistic ESA profile can be interpreted as a mixture of the chlorophyll and the quencher spectra, thus reinforcing our conclusion that a quencher with the features of a carotenoid excited state is needed to explain the observed quenching.

Locating the Quenching Site: The Role of Lutein

Our target model suggests that the quenching mechanism in monomeric CP29 relies on energy transfer from chlorophyll to a carotenoid dark excited state, which we

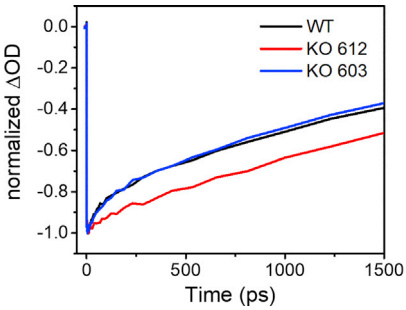

Figure 5. Differences in the Excited-State Relaxation of CP29 WT and Mutants

TA traces recorded at 680 nm for CP29 WT (black), KO612 (red), and KO603 (blue) upon 672 nm excitation. The traces show the decay of negative signal due to ground-state bleaching and excited-state emission in the Qy (see also Figure S18 and Table S1).

assign to S*. The available structures for CP29[24–26] show three distinct carotenoid binding sites: L1, L2, and N1, which bind lutein, violaxanthin, and neoxanthin, respectively (Figure 1). Which of these xanthophylls is responsible for the quenching?

An obvious candidate is a carotenoid located in the proximity of the lowest-energy chlorophylls. It was recently shown that both chlorophylls *a*612 and *a*603 (nomenclature from Pan et al.[26]) are associated with low energy states, implying that CP29 has two terminal emitter domains localized on two different chlorophyll clusters (Figure 1B).[27] Chlorophyll *a*612 is the nearest neighbor of the lutein in site L1, whereas chlorophyll *a*603 is into contact with the violaxanthin in L2 (Figure 1B).[25,26] To investigate the role of these two chlorophyll-carotenoid pairs in the observed quenching mechanism, time-resolved fluorescence was recorded for two CP29 chlorophyll-deficient mutants, namely KO612 and KO603, lacking chlorophyll *a*612 and *a*603, respectively.[27] Time-resolved fluorescence traces measured at room temperature at 680 nm upon 468 nm excitation were satisfactorily fitted with three lifetime components for both mutants (Table 1, second and third rows; Figure S14). The largest contribution (more than 70%) comes from a lifetime component longer than 4 ns. The remaining contributions are from shorter lifetimes, as in the WT (wild type), accounting for fractions of slightly (1.5–2 ns) and strongly quenched (100–200 ps) antennae. As for the shortest lifetime component, KO603 has a very similar lifetime (~100 ps) and amplitude as the WT. On the other hand, the fraction of quenched KO612 complexes has a significantly longer lifetime (around 200 ps) and a smaller amplitude (<10%). In both mutants, global analysis of fluorescence time traces measured at different wavelengths yields very similar DAS for quenched and unquenched components, as already found in CP29 WT (Figures S15–S17). This trend is further confirmed by TA measurements. After 672 nm excitation, the TA traces of CP29 WT and KO603 show a similar fast decaying component (accounting for around 15% of total bleach, black, and blue lines in Figure 5; see Table S1 for details). Such a component is clearly missing in the TA trace of CP29 KO612 (red line in Figure 5; see Figures S18–S19 for further details on TA measurements on CP29 KO612).

These results indicate that the quenching observed in monomeric CP29 WT is conserved in KO603, but it is altered in KO612. We conclude that the carotenoid quenching site active in the monomer of CP29 WT is L1 and thus that the observed carotenoid S* state belongs to lutein, which receives excitation energy mainly from chlorophyll *a*612.

DISCUSSION

Our results show that a heterogeneous model can adequately account for the observed fraction of fluorescence quenching in monomeric CP29 in both

time-resolved fluorescence and TA data. The heterogeneity of the emissive states of LHCs was proposed before on the basis of time-resolved fluorescence measurements[12,31] and demonstrated by single-molecule spectroscopy.[10,11] Single-molecule spectroscopy provided evidence that LHCs can exist in and reversibly switch between quenched and unquenched states, which reflect the vast conformational landscape of these proteins.[5,10] Experiments performed on single LHCs at room temperature have shown that quenched complexes can exhibit emission profiles very similar to those of unquenched complexes, i.e., a major fluorescence band peaking at 680 nm.[4] This is consistent with our observation that quenched and unquenched CP29 monomers show nearly identical fluorescence profiles, suggesting that the quencher is a dark state (such as a carotenoid excited state). By applying a heterogeneous model to our TA data, we were then able to assign the quencher SADS to a carotenoid S* state. Such a mechanism was recently proposed by our group to explain the constitutive quenching observed in LHCII containing astaxanthin instead of the native xanthophylls.[22] In the same work, molecular dynamics simulations suggested that the switch from the light-harvesting to the photoprotective state of a complex might be ascribed to a twist of a carotenoid end-ring, which makes its S* state accessible as energy acceptor from chlorophyll excited states. We speculate that a similar molecular switch might also explain the quenching observed in our sample, with the difference that native xanthophylls inside the isolated CP29 seem to be more prone to remain in a conformation that makes their S* inaccessible, therefore favoring the light-harvesting state of the complex. The tested kinetic scheme is such that the quencher is populated on a slower timescale (60 ps) than its overall lifetime (6 ps), which makes its concentration very small in time (see concentration profiles in Figure S6). This type of kinetics is usually referred as inverted kinetics[41,56] and comes from the fact that the observed quenching rates of LHCs (normally in the order of $[100\ ps]^{-1}$)[7,17,19,22] are much slower than the typical carotenoid lowest-excited-state relaxation rates (in the order of $[10\ ps]^{-1}$).[48] It should be noted that due to the very low concentration of the quencher species, the experimental observation of the described inverted kinetics is extremely challenging, especially at the low excitation powers which are necessary to avoid singlet-singlet annihilation.[17] Chlorophyll to carotenoid energy transfer via an inverted kinetic scheme was observed for the first time in TA experiments performed on LHCII aggregates.[19] Aggregation is indeed known to foster the photoprotective function of antenna complexes.[14,15] However, the excitation power used in those measurements was not low enough to avoid singlet-singlet annihilation, which was later found to possibly produce carotenoid excited states as an artifact.[9] Measuring in annihilation-free conditions is therefore essential to validate any evidence of carotenoid excited-state formation in the observed kinetics. As a result, in this work, much care was devoted to measure below the annihilation threshold, as shown in Text S3 and Figure S20. In this respect, the use of the monomeric protein rather than the aggregate form sets the annihilation threshold to much higher values and represents a valuable ally in experimental terms.

The observed quenching mechanism is very effective, leading to a fluorescence yield that is only 2% of what it is in unquenched complexes (lifetimes drop from 3–4 ns to 60 ps only). The observed lifetime is consequently short enough to efficiently quench photosystem II, helped by the position occupied by CP29 within the supercomplex, i.e., on the energy transfer path from the peripheral antenna to the core complex. Furthermore, a recent work by Valkunas and collaborators[7] has shown that quenching in LHCII aggregates can be explained by a (relatively) small number of quenched monomeric units (with 50–100 ps lifetimes) connected to a larger amount of unquenched complexes. Finally, a lifetime of 150 ps was measured in CP29 crystals.[57]

Quantum mechanical calculations on the structural data suggested that quenching in CP29 crystals is due to chlorophyll to carotenoid energy transfer. It was also shown that, even though all bound xanthophylls can lead to a significant reduction of chlorophyll lifetime, the major effect on quenching can be ascribed to lutein bound to L1, which is in agreement with our results. However, the fact that many chlorophyll-carotenoid couples can potentially contribute to quenching might also explain why removing a specific chlorophyll can reduce the extent of quenching but not suppress it completely. Interestingly, a previous work[58] demonstrated that the spectroscopic properties of the binding site containing chlorophylls *a*611 and *a*612 and lutein 1 are preserved in all LHCs of PSII, which on the basis of the results presented here suggests that a similar quenching mechanism might be active in other antennae.

In conclusion, our data resulting from bulk experiments show that, even in its monomeric form, CP29 can be found in different emissive states, marked by different lifetimes but similar fluorescence spectra. The majority of the complexes is found in a state with a long fluorescence lifetime, which favors the light-harvesting function. However, a small but functionally important fraction of complexes (around 16% of the total) is efficiently quenched by a dark state, which we assign to a carotenoid S* state. Comparison with two chlorophyll-deficient mutants of CP29 suggests that quenching in the WT monomer is due to an energy transfer from chlorophylls to lutein located in the L1 binding site. The observed quenching mechanism is very efficient (lifetime below 100 ps) and is therefore a suitable candidate for non-photochemical quenching in physiological conditions. Finally, the high structural homology between CP29 and other antenna complexes such as LHCII, suggests that this photoprotective strategy can be generalized to other members of the LHC family.

EXPERIMENTAL PROCEDURES

Sample Preparation

Monomeric CP29 and its chlorophyll-deficient mutants were isolated from *Arabidopsis thaliana* as described in Xu et al.[27] For all the measurements, the sample was diluted to the desired OD in a buffer of HEPES 10 mM (pH $\sim$ 7.5) and 0.03% alpha-DM.

Time-Resolved Fluorescence

Time-resolved fluorescence was measured via TCSPC on a FluoTime 200 from PicoQuant at 10°C. The excitation wavelength was 468 nm for all measurements, with a power of 100 μW and a repetition rate of 10 MHz. The OD of all samples was $\leq$0.05. Measurements were performed in a 1x1 cm cuvette and samples were gently stirred. Under these conditions, no power dependency was observed. Signal was acquired at different wavelengths until a number of 20,000 counts at peak maximum, using a time window of 20 ns and a time bin of 4 ps. The instrument response function (IRF), estimated via the measured decay of pinacyanol iodide in methanol (lifetime of around 6 ps[59]), had a full width at half maximum of 88 ps. Fluorescence time traces were globally analyzed using a number of parallel, non-interacting kinetic components, so that the total dataset can be described with the fitting function $F(t,\lambda)$ as follows:

$$F(t,\lambda) = \sum_{k=1}^{n} \mathrm{DAS}_k(\lambda) \cdot \exp\left(-\frac{t}{\tau_k}\right) \otimes \mathrm{IRF}(t,\lambda), \qquad \text{(Equation 1)}$$

where each DAS (DAS_k) is the amplitude factor associated with a decay component k having a decay lifetime τ_k. Fitting quality was assessed by the χ^2 value and by residual inspection.

Ultrafast Transient Absorption Spectroscopy

TA experiments were performed at room temperature on a setup described in more detail elsewhere.[60] In summary, mode-locked pulses centered at 800 nm from a Coherent MIRA seed were amplified by means of regenerative amplification in a Coherent-Rega 9050, where their repetition rate was set to 40 kHz. The Rega output was then split into pump and probe pathways. Optical parametric amplification (Coherent OPA 9400) was employed to tune the wavelength of the pump pulses, which were then narrowed down to a FWHM of 10 nm around their central wavelength via interference filters (THORLABS). Probe pulses were focused into a sapphire crystal to produce a dispersed white-light continuum, which was detected via a 76-channel photodiode array, with a spectral window of around 130 nm. The recorded spectral windows were in the Qx/Qy region (590–720 nm) and in the 480–610 nm region. By changing the pump-pathway length, a delay line allowed recording of TA difference spectra (pumped minus un-pumped) up to 3.5 ns after excitation. Samples were measured at an OD of around 0.8 mm^{-1} at the Qy absorption maximum (678 nm; Figure S4) in a 1 mm Quartz cuvette, and a shaker was used to refresh the sample during the scans. An oxygen scavenging mixture consisting of glucose oxidase 0.1 mg/mL, catalase 0.05 mg/mL, and glucose 10 mM was added to prevent sample degradation (with a HEPES buffer concentration of 50 mM). The pump energy per pulse was set to 5 nJ for 489 nm excitation, 3 nJ for 672 and 682 nm excitation, and 10 nJ for 509 excitation. The amount of annihilation at these pump energies is negligible (see Text S3 and Figure S20, where exhaustive information about the power dependency of the measured signal can be found). The excitation density (calculated as $N_{chl} \times \Delta OD_{max}/2OD_{max}$, where the maxima are restricted to the Qy region and N_{chl} is the number of chlorophylls per monomer) was below 6% of all monomers in all measurements.

Global and target analysis were performed on the TA data matrices as described in van Stokkum et al.[45] Briefly, TA traces recorded simultaneously at different wavelengths were globally analyzed according to Equation 1 to obtain a set of kinetic components, named DADS, representing parallel processes taking place at the excited state with a specific lifetime (as sketched in Figure 3D). The IRF Gaussian profile (FWHM of around 100 fs) was directly estimated from the fitting. A sequential kinetic scheme was also applied to yield so-called EADS, corresponding to the difference spectra of species evolving into the following one (as sketched in Figure 3C) on the same timescales as obtained for DADS. Target analysis was used to extract the difference spectra (species-associated difference spectra [SADS]) of the actual species involved in the measured excited-state kinetics (see van Stokkum et al.[45] for details). Details about the use of spectral equality constraints within the target modeling are given in Text S1. In all global and target analyses, the chirp was explicitly taken into account (by a parametric description of the wavelength-dependent location of the maximum of the IRF).

SUPPLEMENTAL INFORMATION

Supplemental Information can be found online at https://doi.org/10.1016/j.chempr.2019.08.002.

ACKNOWLEDGMENTS

This project was supported by the European Union's Horizon 2020 Research and Innovation Program under the Marie Skłodowska-Curie grant agreement no. 675006 and by the Netherlands Organization for Scientific Research Earth and Life Sciences (NWO-ALW) via a Vici grant to R.C. and a Veni grant to N.L.

AUTHOR CONTRIBUTIONS

Conceptualization, N.L. and R.C.; Methodology, V.M. and N.L.; Investigation, V.M. and N.L.; Resources, P.X. and L.M.R.; Data Analysis, V.M. and I.H.M.v.S.; Writing – Original Draft, V.M. and R.C.; Writing – Review & Editing, V.M., N.L., P.X., L.M.R., I.H.M.v.S., and R.C.; Supervision, R.C. and N.L.

DECLARATION OF INTERESTS

The authors declare no competing interests.

Received: February 2, 2019
Revised: May 18, 2019
Accepted: July 31, 2019
Published: August 29, 2019

REFERENCES AND NOTES

1. Li, X.P., Muller-Moule, P., Gilmore, A.M., and Niyogi, K.K. (2002). PsbS-dependent enhancement of feedback de-excitation protects photosystem II from photoinhibition. Proc. Natl. Acad. Sci. USA *99*, 15222–15227.

2. Kromdijk, J., Głowacka, K., Leonelli, L., Gabilly, S.T., Iwai, M., Niyogi, K.K., and Long, S.P. (2016). Improving photosynthesis and crop productivity by accelerating recovery from photoprotection. Science *354*, 857–861.

3. Pascal, A.A., Liu, Z., Broess, K., van Oort, B., van Amerongen, H., Wang, C., Horton, P., Robert, B., Chang, W., and Ruban, A. (2005). Molecular basis of photoprotection and control of photosynthetic light-harvesting. Nature *436*, 134–137.

4. Krüger, T.P.J., Ilioaia, C., Johnson, M.P., Ruban, A.V., and Van Grondelle, R. (2014). Disentangling the low-energy states of the major light-harvesting complex of plants and their role in photoprotection. Biochim. Biophys. Acta *1837*, 1027–1038.

5. Liguori, N., Periole, X., Marrink, S.J., and Croce, R. (2015). From light-harvesting to photoprotection: structural basis of the dynamic switch of the major antenna complex of plants (LHCII). Sci. Rep. *5*, 15661.

6. Tian, L., Dinc, E., and Croce, R. (2015). LHCII populations in different quenching states are present in the thylakoid membranes in a ratio that depends on the light conditions. J. Phys. Chem. Lett. *6*, 2339–2344.

7. Chmeliov, J., Gelzinis, A., Songaila, E., Augulis, R., Duffy, C.D.P., Ruban, A.V., and Valkunas, L. (2016). The nature of self-regulation in photosynthetic light-harvesting antenna. Nat. Plants *2*, 16045.

8. Barzda, V., Gulbinas, V., Kananavicius, R., Cervinskas, V., Van Amerongen, H., Van Grondelle, R., and Valkunas, L. (2001). Singlet-singlet annihilation kinetics in aggregates and trimers of LHCII. Biophys. J. *80*, 2409–2421.

9. Van Oort, B., Roy, L.M., Xu, P., Lu, Y., Karcher, D., Bock, R., and Croce, R. (2018). Revisiting the role of xanthophylls in nonphotochemical quenching. J. Phys. Chem. Lett. *9*, 346–352.

10. Krüger, T.P.J., Wientjes, E., Croce, R., and van Grondelle, R. (2011). Conformational switching explains the intrinsic multifunctionality of plant light-harvesting complexes. Proc. Natl. Acad. Sci. USA *108*, 13516–13521.

11. Schlau-Cohen, G.S., Yang, H.Y., Krüger, T.P.J., Xu, P., Gwizdala, M., Van Grondelle, R., Croce, R., and Moerner, W.E. (2015). Single-molecule identification of quenched and unquenched states of LHCII. J. Phys. Chem. Lett. *6*, 860–867.

12. Moya, I., Silvestri, M., Vallon, O., Cinque, G., and Bassi, R. (2001). Time-resolved fluorescence analysis of the photosystem II antenna proteins in detergent micelles and liposomes. Biochemistry *40*, 12552–12561.

13. van Oort, B., van Hoek, A., Ruban, A.V., and van Amerongen, H. (2007). Aggregation of light-harvesting complex II leads to formation of efficient excitation energy traps in monomeric and trimeric complexes. FEBS Lett. *581*, 3528–3532.

14. Ruban, A.V., and Horton, P. (1992). Mechanism of ΔpH-dependent dissipation of absorbed excitation energy by photosynthetic membranes. I. Spectroscopic analysis of isolated light-harvesting complexes. Biochim. Biophys. Acta *1102*, 30–38.

15. Horton, P., Wentworth, M., and Ruban, A.V. (2005). Control of the light harvesting function of chloroplast membranes: the LHCII-aggregation model for non-photochemical quenching. FEBS Lett. *579*, 4201–4206.

16. Ilioaia, C., Johnson, M.P., Horton, P., and Ruban, A.V. (2008). Induction of efficient energy dissipation in the isolated light-harvesting complex of photosystem II in the absence of protein aggregation. J. Biol. Chem. *283*, 29505–29512.

17. Müller, M.G., Lambrev, P., Reus, M., Wientjes, E., Croce, R., and Holzwarth, A.R. (2010). Singlet energy dissipation in the photosystem II light-harvesting complex does not involve energy transfer to carotenoids. ChemPhysChem *11*, 1289–1296.

18. Holt, N.E., Zigmantas, D., Valkunas, L., Li, X.P., Niyogi, K.K., and Fleming, G.R. (2005). Carotenoid cation formation and the regulation of photosynthetic light harvesting. Science *307*, 433–436.

19. Ruban, A.V., Berera, R., Ilioaia, C., van Stokkum, I.H.M., Kennis, J.T.M., Pascal, A.A., Van Amerongen, H., Robert, B., Horton, P., and Van Grondelle, R. (2007). Identification of a mechanism of photoprotective energy dissipation in higher plants. Nature *450*, 575–578.

20. Bode, S., Quentmeier, C.C., Liao, P.N., Hafi, N., Barros, T., Wilk, L., Bittner, F., and Walla, P.J. (2009). On the regulation of photosynthesis by excitonic interactions between carotenoids and chlorophylls. Proc. Natl. Acad. Sci. USA *106*, 12311–12316.

21. Staleva, H., Komenda, J., Shukla, M.K., Šlouf, V., Kaňa, R., Polívka, T., and Sobotka, R. (2015). Mechanism of photoprotection in the cyanobacterial ancestor of plant antenna proteins. Nat. Chem. Biol. *11*, 287–291.

22. Liguori, N., Xu, P., van Stokkum, I.H.M., Van Oort, B., Lu, Y., Karcher, D., Bock, R., and Croce, R. (2017). Different carotenoid conformations have distinct functions in light-harvesting regulation in plants. Nat. Commun. *8*, 1994.

23. Dolganov, N.A.M., Bhaya, D., and Grossman, A.R. (1995). Cyanobacterial protein with similarity to the chlorophyll a/b binding proteins of higher plants: evolution and regulation. Proc. Natl. Acad. Sci. USA *92*, 636–640.

24. Wei, X., Su, X., Cao, P., Liu, X., Chang, W., Li, M., Zhang, X., and Liu, Z. (2016). Structure of spinach photosystem II – LHCII supercomplex at 3.2 Å resolution. Nature *534*, 69–74.

25. Su, X., Wei, X., Zhu, D., Chang, W., and Liu, Z. (2017). Structure and assembly mechanism of plant C2S2M2-type PSII-LHCII supercomplex. Science *820*, 815–820.

26. Pan, X., Li, M., Wan, T., Wang, L., Jia, C., Hou, Z., Zhao, X., Zhang, J., and Chang, W. (2011). Structural insights into energy regulation of light-harvesting complex CP29 from spinach. Nat. Struct. Mol. Biol. *18*, 309–315.

27. Xu, P., Roy, L.M., and Croce, R. (2017). Functional organization of photosystem II antenna complexes: CP29 under the spotlight. Biochim. Biophys. Acta. Bioenerg. *1858*, 815–822.

28. de Bianchi, S., Betterle, N., Kouril, R., Cazzaniga, S., Boekema, E., Bassi, R., and Dall'Osto, L. (2011). Arabidopsis mutants deleted in the light-harvesting protein Lhcb4 have a disrupted photosystem II macrostructure and are defective in photoprotection. Plant Cell *23*, 2659–2679.

29. Miloslavina, Y., De Bianchi, S., Dall'Osto, L., Bassi, R., and Holzwarth, A.R. (2011). Quenching in Arabidopsis thaliana mutants lacking monomeric antenna proteins of photosystem II. J. Biol. Chem. *286*, 36830–36840.

30. Mullineaux, C.W., Pascal, A.A., Horton, P., and Holzwarth, A.R. (1993). Excitation-energy quenching in aggregates of the LHC II chlorophyll-protein complex: a time-resolved fluorescence study. Biochim. Biophys. Acta - Bioenerg. *1141*, 23–28.

31. Passarini, F., Wientjes, E., van Amerongen, H., and Croce, R. (2010). Photosystem I light-harvesting complex Lhca4 adopts multiple conformations: red forms and excited-state quenching are mutually exclusive. Biochim. Biophys. Acta *1797*, 501–508.

32. Miloslavina, Y., Wehner, A., Lambrev, P.H., Wientjes, E., Reus, M., Garab, G., Croce, R., and Holzwarth, A.R. (2008). Far-red fluorescence: a direct spectroscopic marker for LHCII oligomer formation in non-photochemical quenching. FEBS Lett. *582*, 3625–3631.

33. Farooq, S., Chmeliov, J., Wientjes, E., Koehorst, R., Bader, A., Valkunas, L., Trinkunas, G., and Van Amerongen, H. (2018). Dynamic feedback of the photosystem II reaction centre on photoprotection in plants. Nat. Plants *4*, 225–231.

34. Van Oort, B., Van Hoek, A., Ruban, A.V., and Van Amerongen, H. (2007). Equilibrium between quenched and nonquenched conformations of the major plant light-harvesting complex studied with high-pressure time-resolved fluorescence. J. Phys. Chem. B *111*, 7631–7637.

35. Kondo, T., Pinnola, A., Chen, W.J., Dall'Osto, L., Bassi, R., and Schlau-Cohen, G.S. (2017). Single-molecule spectroscopy of LHCSR1 protein dynamics identifies two distinct states responsible for multi-timescale photosynthetic photoprotection. Nat. Chem. *9*, 772–778.

36. Gruber, J.M., Xu, P., Chmeliov, J., Krüger, T.P.J., Alexandre, M.T.A., Valkunas, L., Croce, R., and Van Grondelle, R. (2016). Dynamic quenching in single photosystem II supercomplexes. Phys. Chem. Chem. Phys. *18*, 25852–25860.

37. Natali, A., Gruber, J.M., Dietzel, L., Stuart, M.C.A., Van Grondelle, R., and Croce, R. (2016). Light-harvesting complexes (LHCs) cluster spontaneously in membrane environment leading to shortening of their excited state lifetimes. J. Biol. Chem. *291*, 16730–16739.

38. Akhtar, P., Görföl, F., Garab, G., and Lambrev, P.H. (2019). Dependence of chlorophyll fluorescence quenching on the lipid-to-protein ratio in reconstituted light-harvesting complex II membranes containing lipid labels. Chem. Phys. *522*, 242–248.

39. Gruber, J.M., Scheidelaar, S., van Roon, H., Dekker, J.P., Killian, J.A., and van Grondelle, R. (2016). Photophysics in single light-harvesting complexes II: from micelle to native nanodisks. In Proceedings of Single Molecule Spectroscopy and Superresolution Imaging IX, p. 9714.

40. Belgio, E., Johnson, M.P., Jurić, S., and Ruban, A.V. (2012). Higher plant photosystem II light-harvesting antenna, not the reaction center, determines the excited-state lifetime - both the maximum and the nonphotochemically quenched. Biophys. J. *102*, 2761–2771.

41. Berera, R., Van Grondelle, R., and Kennis, J.T.M. (2009). Ultrafast transient absorption spectroscopy: principles and application to photosynthetic systems. Photosynth. Res. *101*, 105–118.

42. Croce, R., Müller, M.G., Bassi, R., and Holzwarth, A.R. (2003). Chlorophyll b to chlorophyll a energy transfer kinetics in the CP29 antenna complex: a comparative femtosecond absorption study between native and reconstituted proteins. Biophys. J. *84*, 2508–2516.

43. Salverda, J.M., Vengris, M., Krueger, B.P., Scholes, G.D., Czarnoleski, A.R., Novoderezhkin, V., Van Amerongen, H., and Van Grondelle, R. (2003). Energy transfer in light-harvesting complexes LHCII and CP29 of spinach studied with three pulse echo peak shift and transient grating. Biophys. J. *84*, 450–465.

44. Mozzo, M., Dall'Osto, L., Hienerwadel, R., Bassi, R., and Croce, R. (2008). Photoprotection in the antenna complexes of photosystem II. Role of individual xanthophylls in chlorophyll triplet quenching. J. Biol. Chem. *283*, 6184–6192.

45. van Stokkum, I.H.M., Larsen, D.S., and Van Grondelle, R. (2004). Global and target analysis of time-resolved spectra. Biochim. Biophys. Acta *1657*, 82–104.

46. Croce, R., Müller, M.G., Caffarri, S., Bassi, R., and Holzwarth, A.R. (2003). Energy transfer pathways in the minor antenna complex CP29 of photosystem II: a femtosecond study of carotenoid to chlorophyll transfer on mutant and WT complexes. Biophys. J. *84*, 2517–2532.

47. Niedzwiedzki, D.M., Sullivan, J.O., Polívka, T., Birge, R.R., and Frank, H.A. (2006). Femtosecond time-resolved transient absorption spectroscopy of xanthophylls. J. Phys. Chem. B *110*, 22872–22885.

48. Polívka, T., and Sundström, V. (2004). Ultrafast dynamics of carotenoid excited states—from solution to natural and artificial systems. Chem. Rev. *104*, 2021–2071.

49. Papagiannakis, E., Kennis, J.T.M., van Stokkum, I.H.M., Cogdell, R.J., and Van Grondelle, R. (2002). An alternative carotenoid-to-bacteriochlorophyll energy transfer pathway in photosynthetic light harvesting. Proc. Natl. Acad. Sci. USA *99*, 6017–6022.

50. Papagiannakis, E., Das, S.K., Gall, A., van Stokkum, I.H.M., Robert, B., van Grondelle, R., Frank, H.A., and Kennis, J.T.M. (2003). Light harvesting by carotenoids incorporated into the B850 light-harvesting complex from *Rhodobacter s phaeroides* R-26.1: excited-state relaxation, ultrafast triplet formation, and energy transfer to bacteriochlorophyll. J. Phys. Chem. B *107*, 5642–5649.

51. Larsen, D.S., Papagiannakis, E., van Stokkum, I.H.M., Vengris, M., Kennis, J.T.M., and Van Grondelle, R. (2003). Excited state dynamics of b -carotene explored with dispersed multi-pulse transient absorption. Chem. Phys. Lett. *381*, 733–742.

52. Polívka, T., and Sundström, V. (2009). Dark excited states of carotenoids: consensus and controversy. Chem. Phys. Lett. *477*, 1–11.

53. Niedzwiedzki, D., Koscielecki, J.F., Cong, H., Sullivan, J.O., Gibson, G.N., Birge, R.R., and Frank, H.A. (2007). Ultrafast dynamics and excited state spectra of open-chain carotenoids at room and low temperatures. J. Phys. Chem. B *111*, 5984–5998.

54. Cong, H., Niedzwiedzki, D.M., Gibson, G.N., and Frank, H.A. (2008). Ultrafast time-resolved spectroscopy of xanthophylls at low temperature. J. Phys. Chem. B *112*, 3558–3567.

55. Van Oort, B., Van Grondelle, R., and van Stokkum, I.H.M. (2015). A hidden state in light-harvesting complex II revealed by multipulse spectroscopy. J. Phys. Chem. B *119*, 5184–5193.

56. Berera, R., Herrero, C., van Stokkum, I.H.M., Vengris, M., Kodis, G., Palacios, R.E., van Amerongen, H., van Grondelle, R., Gust, D., Moore, T.A., et al. (2006). A simple artificial light-harvesting dyad as a model for excess energy dissipation in oxygenic photosynthesis. Proc. Natl. Acad. Sci. USA *103*, 5343–5348.

57. Fox, K.F., Ünlü, C., Balevičius, V., Ramdour, B.N., Kern, C., Pan, X., Li, M., van Amerongen, H., and Duffy, C.D.P. (2018). A possible molecular basis for photoprotection in the minor antenna proteins of plants. Biochim. Biophys. Acta - Bioenerg. *1859*, 471–481.

58. Mozzo, M., Passarini, F., Bassi, R., van Amerongen, H., and Croce, R. (2008). Photoprotection in higher plants: the putative quenching site is conserved in all outer light-harvesting complexes of photosystem II. Biochim. Biophys. Acta *1777*, 1263–1267.

59. Van Oort, B., Amunts, A., Borst, J.W., Van Hoek, A., Nelson, N., Van Amerongen, H., and Croce, R. (2008). Picosecond fluorescence of intact and dissolved PSI-LHCI crystals. Biophys. J. *95*, 5851–5861.

60. Liguori, N., Novoderezhkin, V., Roy, L.M., Van Grondelle, R., and Croce, R. (2016). Excitation dynamics and structural implication of the stress-related complex LHCSR3 from the green alga Chlamydomonas reinhardtii. Biochim. Biophys. Acta *1857*, 1514–1523.

Chem, Volume *5*

Supplemental Information

Capturing the Quenching Mechanism of Light-Harvesting Complexes of Plants by Zooming in on the Ensemble

Vincenzo Mascoli, Nicoletta Liguori, Pengqi Xu, Laura M. Roy, Ivo H.M. van Stokkum, and Roberta Croce

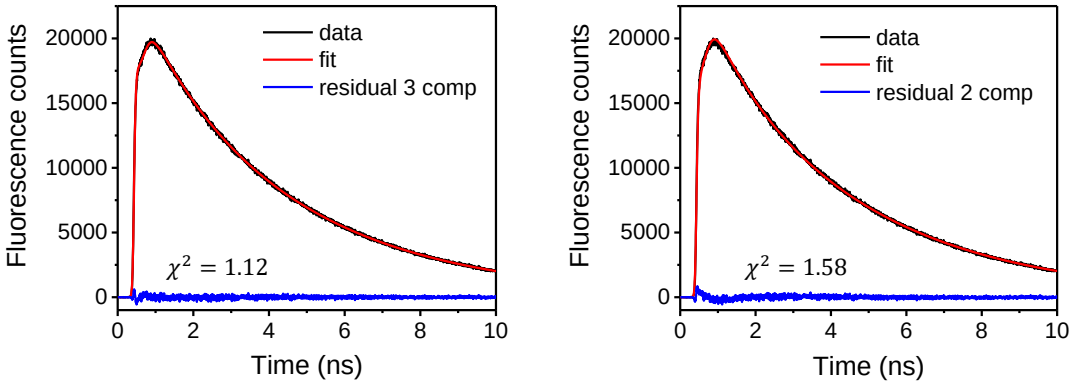

Figure S1. Time-resolved fluorescence experiments on CP29 WT (related to Table 1). Measured (in black) and fitted (in red) fluorescence time traces at 680 nm for CP29 WT upon 468 nm excitation. The difference between measured and fitted data (residuals) is displayed in blue. The left panel shows the 3-component fitting presented in the main text with the relative χ^2. The right panel shows a 2 component fitting for comparison (corresponding to a 84% component of 3.99 ns lifetime and a 16% component with 1.04 lifetime). A 3-component fitting results in significantly lower χ^2 and less structured residuals, implying that 3 components are necessary for a satisfactory fitting.

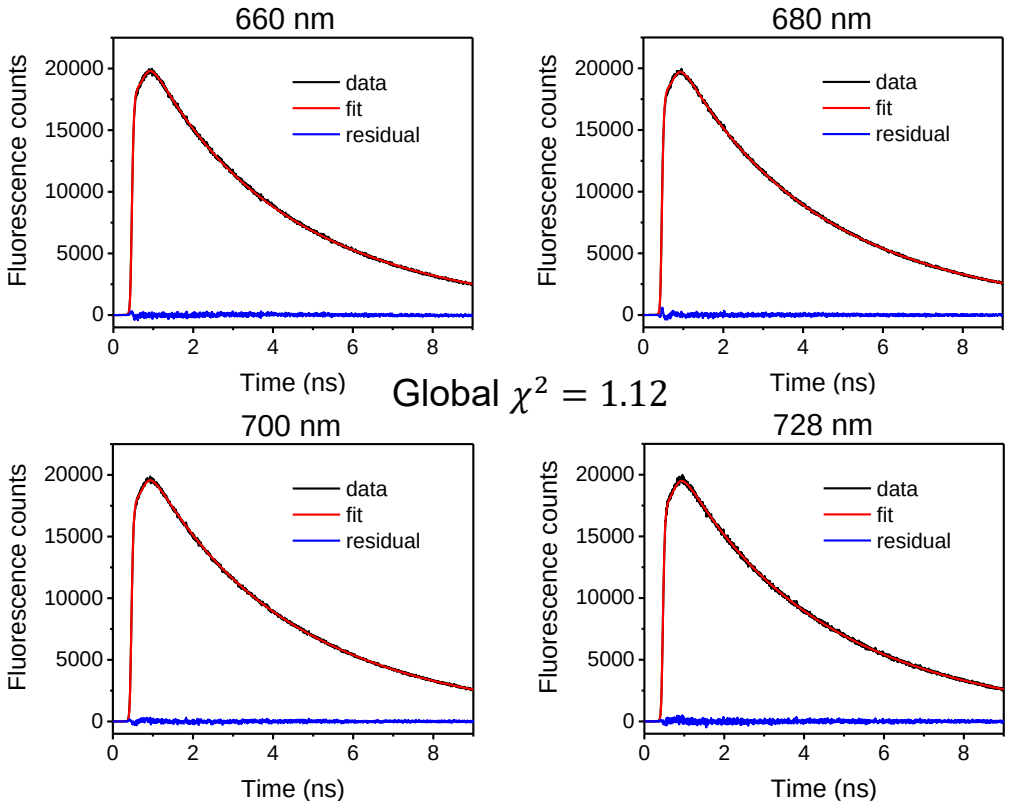

Figure S2. Time-resolved fluorescence experiments on CP29 WT at multiple wavelengths (related to Figure 2). Measured (in black) and fitted (in red) fluorescence time traces at selected wavelengths for CP29 WT upon 468 nm excitation. Residuals are displayed in blue.

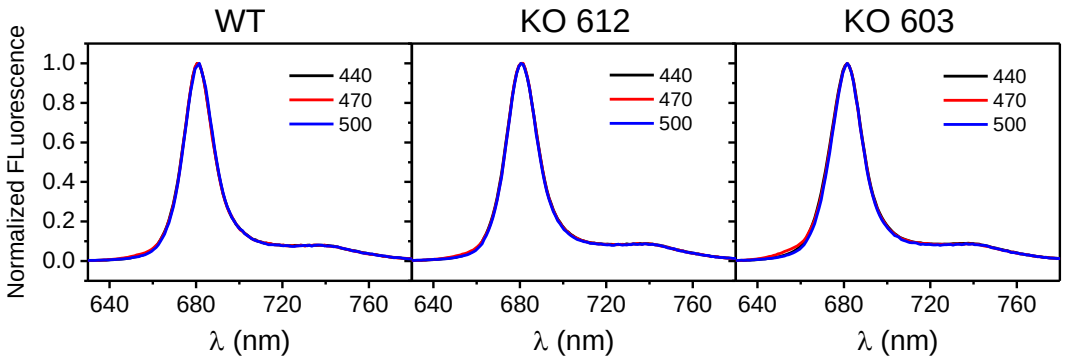

Figure S3. Steady-state fluorescence experiments. Steady-state fluorescence spectra of CP29 WT (left), KO612 (middle) and KO603 (right) for preferential chlorophyll a (440 nm, black line), chlorophyll b (470 nm, red line) and carotenoid (500 nm, blue line) excitation. The emission spectra of CP29 WT and KO603 peak at 681.5 nm, that of CP29 KO612 at 681 nm.

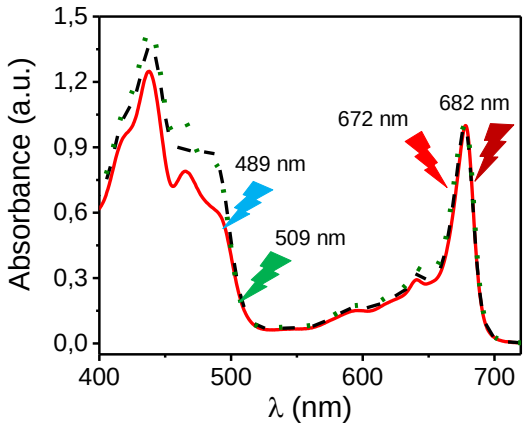

Figure S4. Steady-state absorption experiments. Absorption spectra of CP29 WT (red solid line), KO612 (black dashed) and KO603 (green dotted). The lightning bolts indicate the different excitation wavelengths for TA experiments (see methods in the main text).

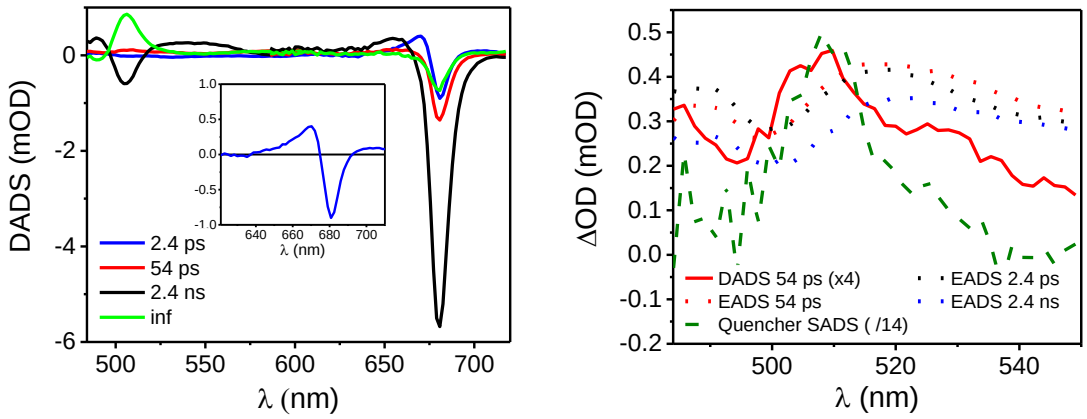

Figure S5. Global analysis of transient absorption experiments (related to Figure 3E-F). Left: DADS from global analysis of TA data upon 682 nm excitation of CP29 WT. The inset shows a magnification of the 2.4 ps DADS in the Qy region. Due to its bandshift feature, it can be assigned to a chlorophyll-chlorophyll uphill energy equilibration. Right: overlay of chlorophyll ESA profiles from 2.4 ps, 54 ps, and 2.4 ns EADS in Figure 3C-E of the manuscript (black, red and blue dotted lines) and the 54 ps DADS (multiplied by a factor of 4 for better comparison) from the DADS shown in the left panel. The quencher SADS as obtained from the heterogeneous target model presented in the main text is also shown for comparison (scaled by a factor of 14, green dashed line). The 54 ps DADS can be interpreted as a superposition of a typical chlrophyll spectrum with that of the quencher.

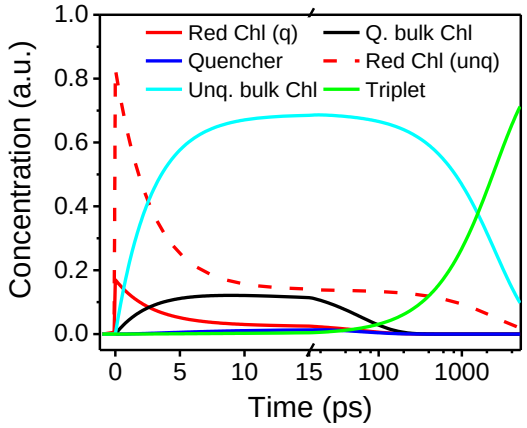

Figure S6. Results from the heterogeneous target model (related to Figure 4). Concentration profiles for the 6 species in the heterogeneous target model in the main text (see Figure 4A for the compartment kinetic model and Figure 4B for the SADS). Please note that the time axis is linear until 15 ps and logarithmic thereafter. The maximum of the quencher concentration is 0.013 at 20 ps. The same concentration profiles are also obtained for the above-mentioned alternative set of equality constraints, since the fitted kinetics are virtually unchanged.

Text S1. Details about the compartmental model and the equality constraints

As explained in the main text, the TA data for the 682 nm excitation experiment are modeled via a target compartmental scheme. The heterogeneity of the system is described by introducing two parallel schemes (each containing three compartments), representing unquenched/quenched complexes. More specifically, energy equilibration in the Qy region is described by an equilibrium between 2 pools of chlorophylls, a pre-equilibrated (red) pool representing the initial excitation of the 682 nm pulse and an equilibrated bulk pool. In order to simplify the kinetic modeling and reduce the number of free parameters, the spectra of the pre-equilibrated chlorophylls are assumed to be the same in the unquenched and quenched complexes. Both forward and backward rates of equilibration between red chlorophylls and bulk chlorophylls are also equated in quenched and unquenched CP29 (see arrows between red and black/cyan compartments in Figure 4A). These assumptions are justified by the evidence that the terminal emitter domain of quenched and unquenched complexes is unchanged (see also fluorescence data), suggesting that energy equilibration in the Qy is similar in both emissive states.

The weak signal in the chlorophyll Excited State Absorption (ESA) region required the use of equality constraints for the shapes of the chlorophyll SADS at wavelengths shorter than 630 nm. Different sets of constraints were therefore tested based on the same heterogeneous model schematized in Figure 4A of the main text. The main difference in these models is in the fitting quality in the region of chlorophyll ESA and in the shape of the resulting quencher spectrum, whereas the spectra of the triplet state and of all chlorophyll species in the Qy are insensitive to the different constraints. Due to the relatively low contribution of the signal in the chlorophyll ESA region to the overall residuals, the fitting quality was assessed not only by the total residual standard error, but also by visual inspection of the fitted and measured time traces. It is important to notice that all these models, despite some spectral changes, consistently result in a quencher SADS with typical features of a carotenoid excited state (i.e., a bleach below 500 nm and a positive difference absorption in the region between 500 and 560 nm).

The model which resulted in the best fitting quality (lower error and better reproduction of the signal in the chlorophyll ESA region, Figure S3) assumes that the ESA of red and bulk quenched chlorophylls (red and black compartments in Figure 4A) are equal, while the shapes of the ESA of unquenched bulk chlorophylls (cyan compartment) can differ slightly. The SADS for the described model are shown in Figure 4B (main text). A different set of equality constraints, where the ESA of quenched and unquenched chlorophylls are equated but can differ from that of red pre-equilibrated chlorophylls, gives almost identical result (data not shown). Another model, which equates the ESA profile of all chlorophyll species (red, black and cyan compartments in Figure 4A) yields a less satisfactory fitting, but it is shown below for completeness. The aforementioned equality constraints are more restrictive than those adopted in the model presented in the main text and, as a result, a lower fitting quality is achieved. As discussed previously, the fitting is not affected in the Qy region, where the largest part of the total signal is recorded. As a result, the kinetic rates are essentially the same as those obtained for the model shown in the main text (see Figure 4A). Moreover, the resulting fitting is, overall, almost as accurate as for the previous model (see Figure S7 and S8 for an overlay of fitted/measured data). However, even if the total residual error increases by only 0.5%, the fitting quality is significantly less satisfactory in the region between 530 nm and 560 nm (see Figure S9 to compare the different fitting qualities in this region). This new set of constraints also results in a different quencher spectrum (Figure S10), with a broad positive signal peaking around 530 nm and a strong bleach below 500 nm. This spectrum is significantly red-shifted and broader compared to the quencher spectrum shown in the main text but preserves typical features of a carotenoid singlet excited state. The peak position is also closer to the region where S_1 ESA is expected (see Figure 4C in the main text). However, the quencher spectrum is still blue-shifted compared to the CP29-bound lutein S_1 ESA spectrum (whose peak should be around 550 nm as previously measured[46]) and, even compared to the S_1 ESA spectrum of violaxanthin, it is broader and exhibits significantly more amplitude in the region at shorter wavelengths than the main peak. This evidence supports again the hypothesis that the quencher can be assigned to a carotenoid S* state. Anyway, the quencher spectrum going below zero above 570 nm and the lower fitting quality make this model less realistic than the one shown in the main text.

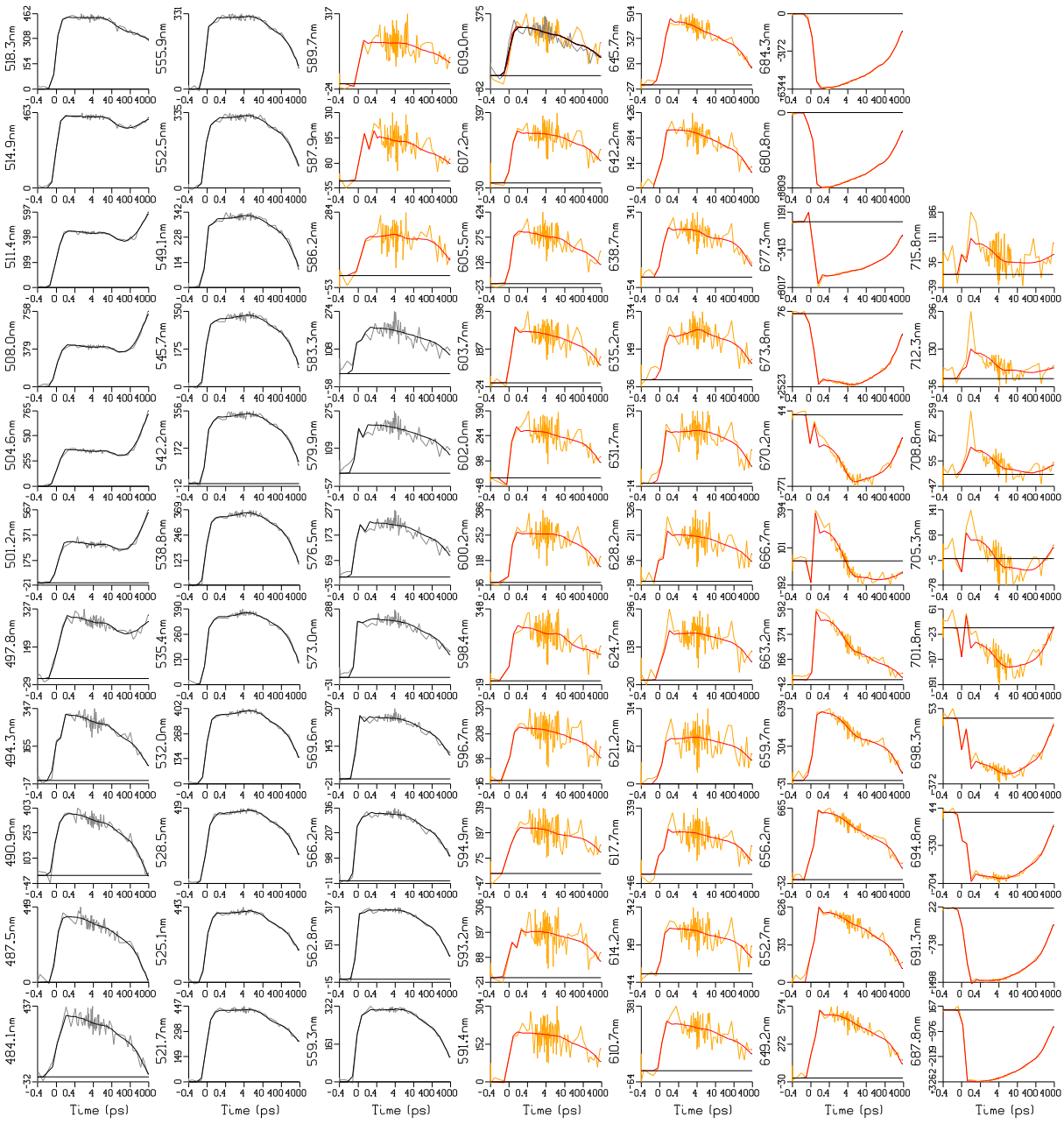

Figure S7. Transient absorption data and fitting (related to Figure 3). Time traces of raw data (light colors, in µOD) and fit (dark colors) with the equality constraints adopted in the main text (ESA profile of bulk unquenched chlorophyll compartment different from ESA profiles of other chlorophyll compartments). This is also the fitting yielding the best fit quality. Wavelength is indicated in the ordinate label of each panel. Please note that the time scale is linear until 0.4 ps and logarithmic thereafter. Please note that each panel is scaled to its maximum and all the time zeroes (location of the maximum of the IRF) are chirp corrected.

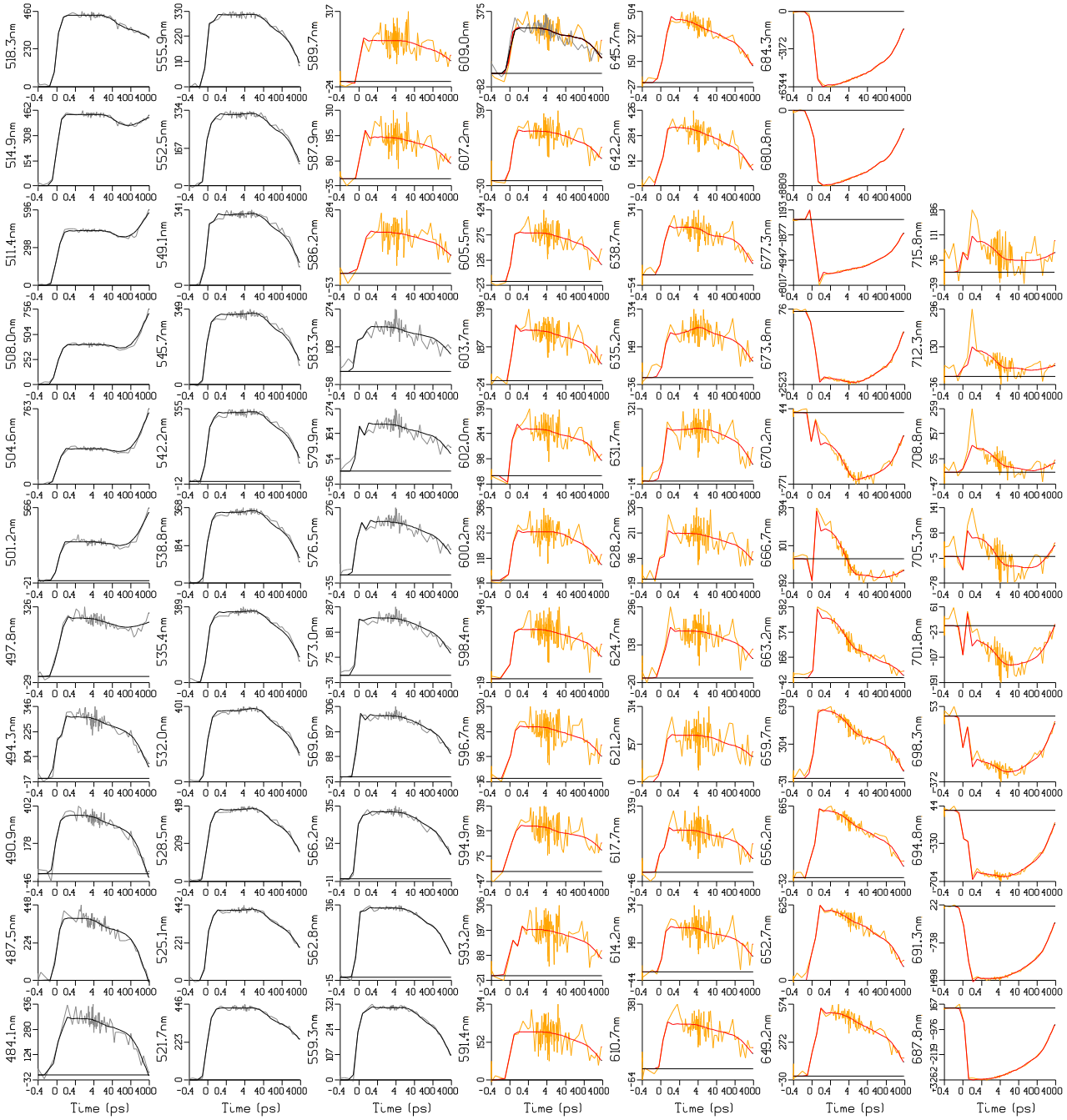

Figure S8. Transient absorption data and fitting: alternative equality constraints. Time traces of raw data (light colors, in μOD) and fit (dark colors) with the alternative equality constraints adopted in the Supplemental Information, Text S1 (ESA profile of all chlorophyll species forced to be equal). Wavelength is indicated in the ordinate label of each panel. Please note that the time scale is linear until 0.4 ps and logarithmic thereafter. Please note that each panel is scaled to its maximum and all the time zeroes (location of the maximum of the IRF) are chirp corrected.

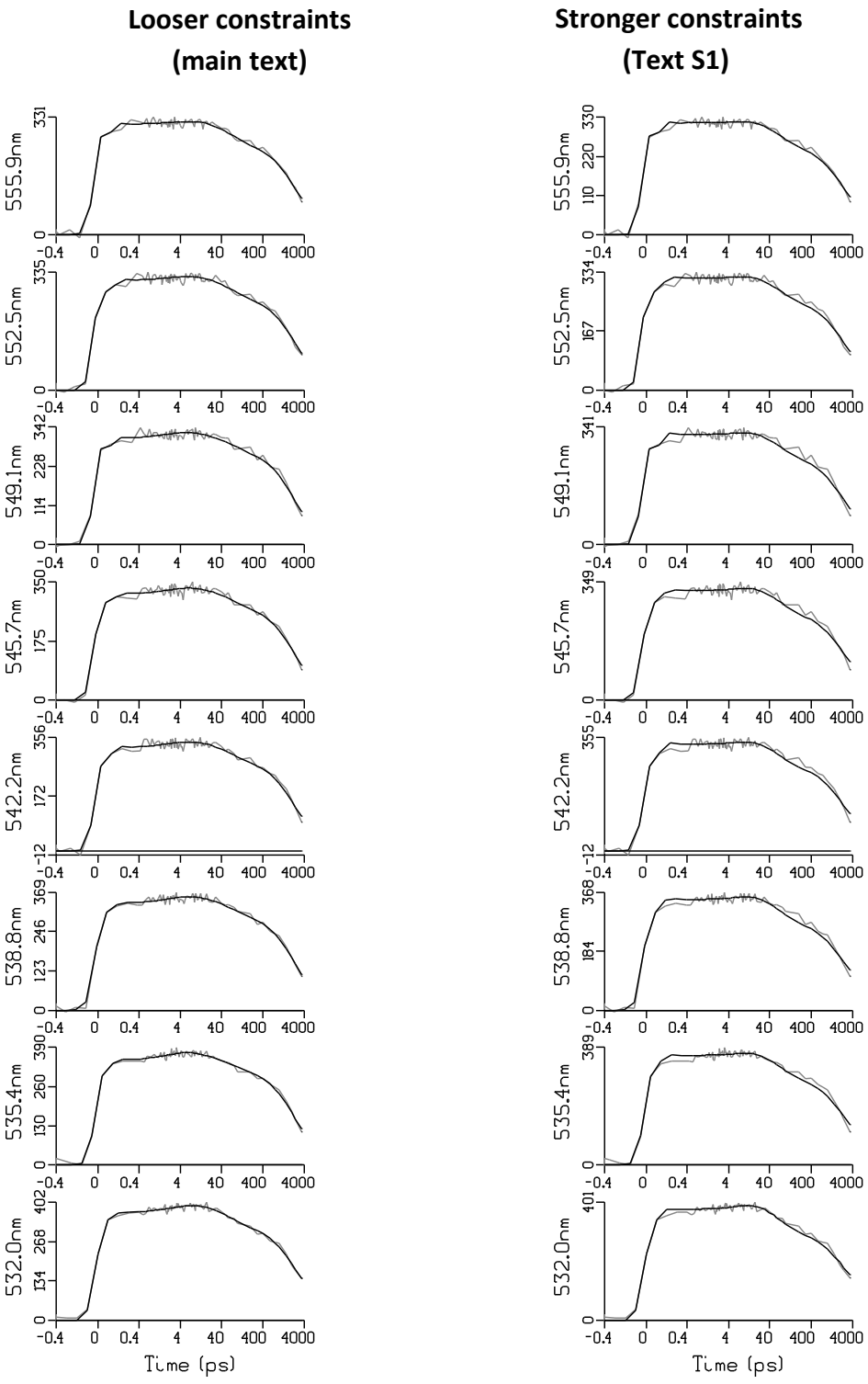

Figure S9. Transient absorption data and fitting: comparing different constraints. Zoom in of the experimental (light colors) and fit (dark color) traces between 532 nm and 556 nm, already shown in Figure S7 and S8. The left panel is referred to the set of equality constraints presented in the main text (leading to the best fitting). The right panel is referred to the alternative set of constraints presented in the Supplemental Information, Text S1.

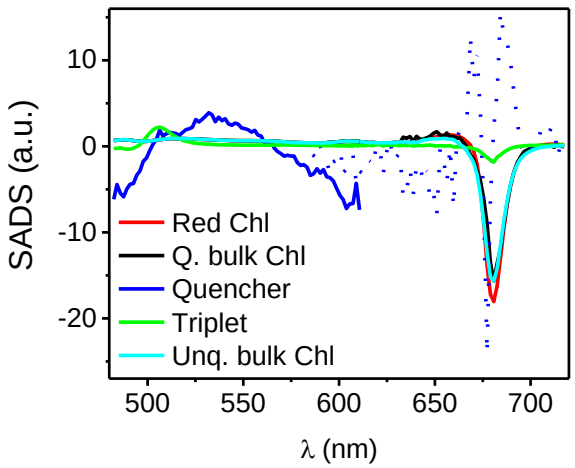

Figure S10. Alternative constraints on the target model (related to Figure 4A,B). Species associated decay spectra (SADS) of each compartment in the target model of Figure 4A in the main text, but using more restrictive equality constraints (all chlorophyll spectra equal at wavelengths shorter than 630 nm). The quencher spectrum in the Qy is depicted as a dotted line to allow better visualization of the chlorophyll spectra.

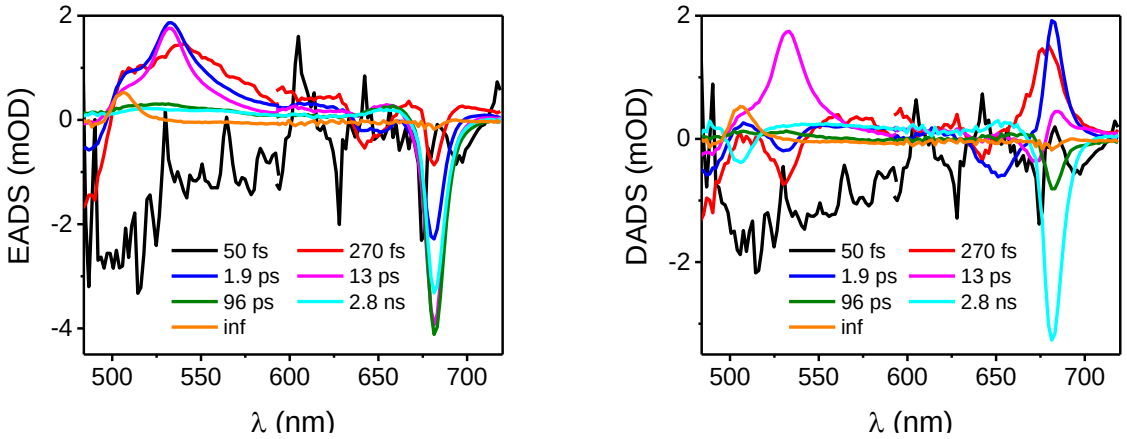

Figure S11. Transient absorption experiments upon carotenoid excitation. Evolution Associated Difference Spectra (EADS, left panel) and Decay Associated Difference Spectra (DADS, right panel) for the 489 nm excitation TA experiment on CP29 WT. The pump preferentially excites the carotenoid S_2 state, marked by a strong bleach in the high energy region (black EADS). This state quickly decays (the lifetime of 50 fs was fixed being at the limit of the experimental time resolution) to a lower energy carotenoid state (red EADS). At the same time, some bleach appears in the Qy region, implying that the carotenoid S_2 state transfers energy to the chlorophylls. The red EADS in the high energy region represents excited state absorption (ESA) from the vibrationally excited ("hot") S_1 state of carotenoids. Such state relaxes in about 0.3 ps to the S_1 state (blue EADS). At the same time, some extra bleach is formed in the Qy region and some energy transfer from chlorophyll b to chlorophyll a is also observed. Some further chlorophyll b/a equilibration takes place in 1.9 ps (blue to magenta EADS and blue DADS). The carotenoid S_1 state decays in 13 ps (magenta to green EADS, magenta DADS), without major changes in the Qy bleaching (magenta and green EADS nearly overlap in the Qy), meaning that the efficiency of energy transfer from the carotenoid S_1 state to the chlorophylls is low (if any). The remaining Qy bleach due to chlorophyll excited states relaxes with 96 ps and 2.8 ns time constants (stemming from quenched and unquenched CP29, green to cyan and cyan to orange EADS) and finally populates long-lived triplet states (orange EADS). These results are consistent with previous TA measurements on CP29[46]. The magenta DADS in the high energy region, peaking at 532 nm (lifetime of 13 ps), can be assumed to represent the spectrum of the carotenoid S_1 (Figure 4C in the main text). A previous study[46] demonstrated that this signal is originated from the carotenoid bound to the L2 site, i.e. violaxanthin (its shape and width are also compatible with that of the S_1 of violaxanthin in solution[47]). Such a signal might also contain smaller contributions from lutein and neoxanthin S_1 ESAs, which are expected to peak at even longer wavelengths (above 540-550 nm)[46,47]. Excitation at 509 nm results in very similar excited state dynamics, as well as direct carotenoid excitation in the mutants (data not shown).

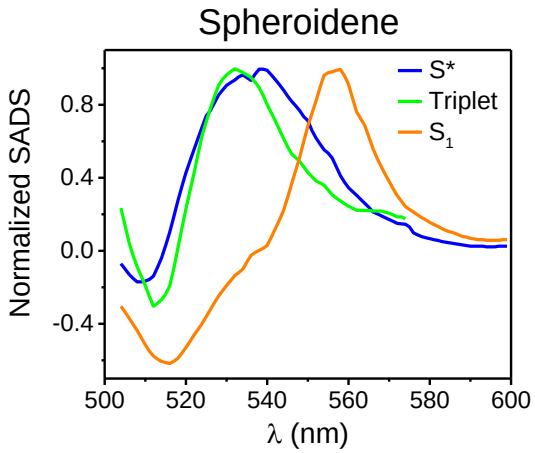

Figure S12. Carotenoid excited state spectra (related to Figure 4C). SADS for spheroidene S*, triplet and S_1 states from TA experiments on LH2 of *Rb. Sphaeroides*[49]. Similarly to what observed for the quencher SADS in CP29 (see Figure 4C in the main text), the S* spectrum exhibits a good overlap with the triplet spectrum and is significantly blue-shifted in comparison to the S_1 spectrum.

Text S2. Details about the wiggling feature in the Qy for the quencher spectrum

The quencher SADS shows a wiggling feature in the Qy region (blue SADS in Figure 4B, main text, and in Figure S10 for the alternative model). However, the signal to noise ratio in this spectral region is significantly worse than below 600 nm, where the carotenoid-resembling feature is present. A similar feature in the Qy was previously observed[22,55] and ascribed to coupling of Chlorophyll Qy transitions to the carotenoid excited state. However, we cannot exclude that such a signal arises from some minor slower energy transfer dynamics between chlorophylls which is not captured by the single equilibration step included in the model. It must be noted, however, that due to the very low concentration of the quencher and the large absolute signal in the Qy, the relative contribution of this signal to the Qy dynamics is practically negligible. On the other hand, the contribution of the quencher spectrum has a significant weight in the dynamics in the high energy region (480-570 nm).

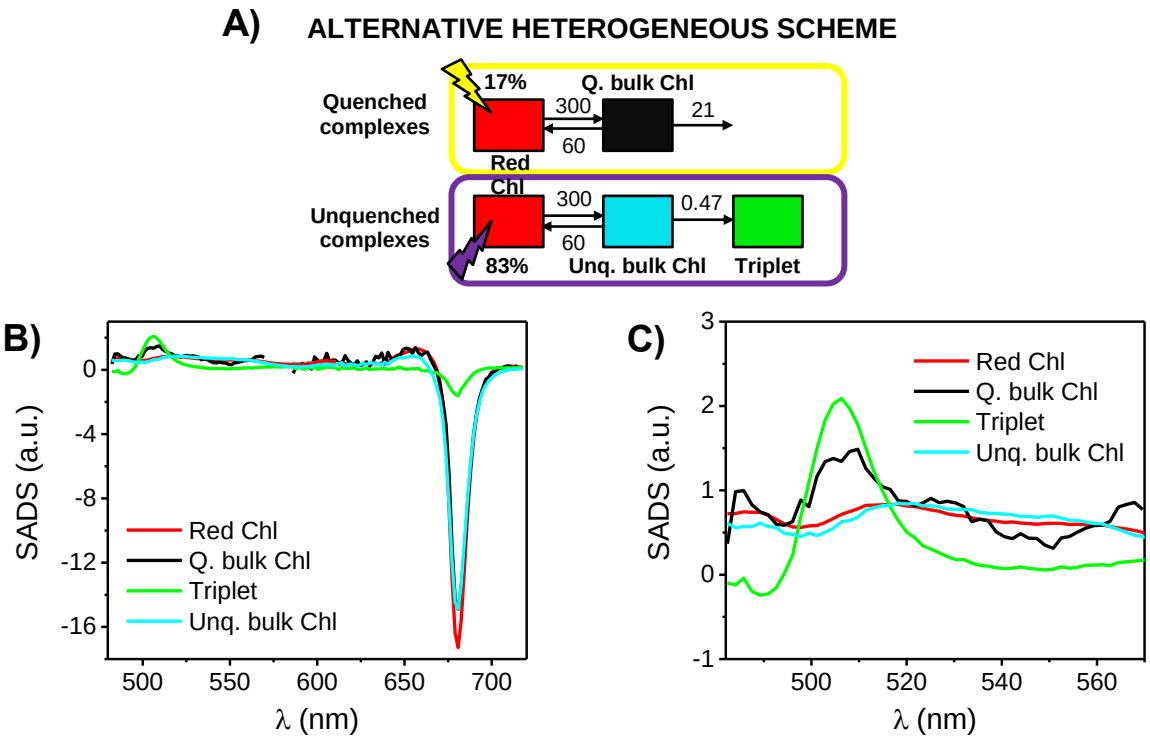

Figure S13. Alternative heterogeneous model without quencher (related to Figure 4). A) Alternative heterogeneous target scheme for the 682 nm excitation TA data of CP29 lacking the quencher compartment (i.e., quenched chlorophyll relaxes to the ground state directly). The model yields very similar kinetic rates as obtained from the heterogeneous kinetic model presented in the manuscript (i.e. with the addition of the quencher compartment, see Figure 4). B) SADS obtained from the scheme shown on top. C) expansion of ESA (excited state absorption) profiles of SADS shown in panel B). The quenched chlorophyll ESA profile (black SADS) exhibits a peak overlapping with the triplet spectrum and its shape is markedly different from that of the other chlorophyll species.

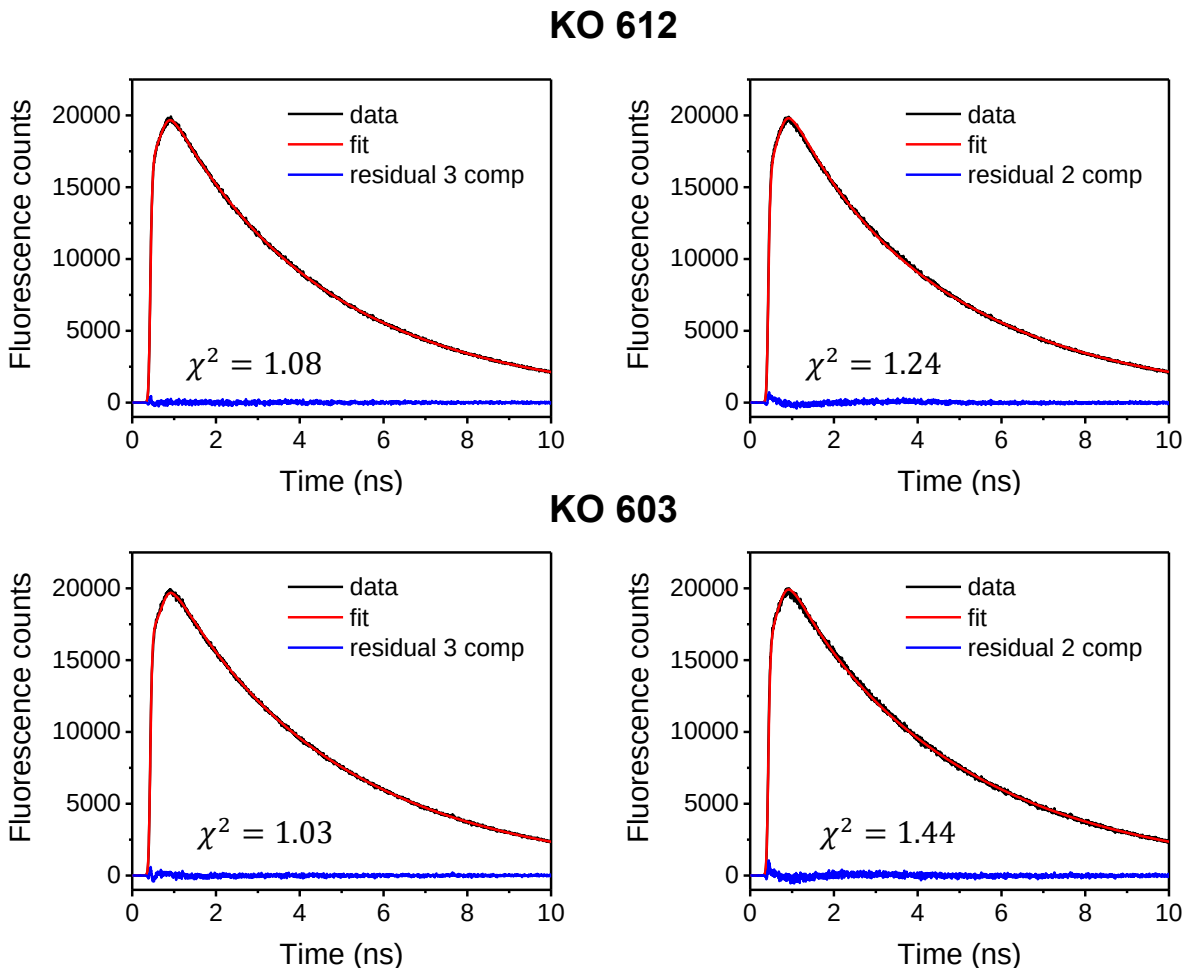

Figure S14. Time-resolved fluorescence experiments on CP29 mutants (related to Table 1). Measured (in black) and fitted (in red) fluorescence time traces at 680 nm for CP29 KO612 (top) and KO603 (bottom) upon 468 nm excitation. The difference between measured and fitted data (residuals) is displayed in blue. The left panels show the 3-component fitting presented in the main text with the relative χ^2. The right panels show a 2 component fitting for comparison. A 3-component fitting results in significantly lower χ^2 and less structured residuals, especially for CP29 KO603 (in a similar way as in the WT), implying that 3 components are necessary for a satisfactory fitting.

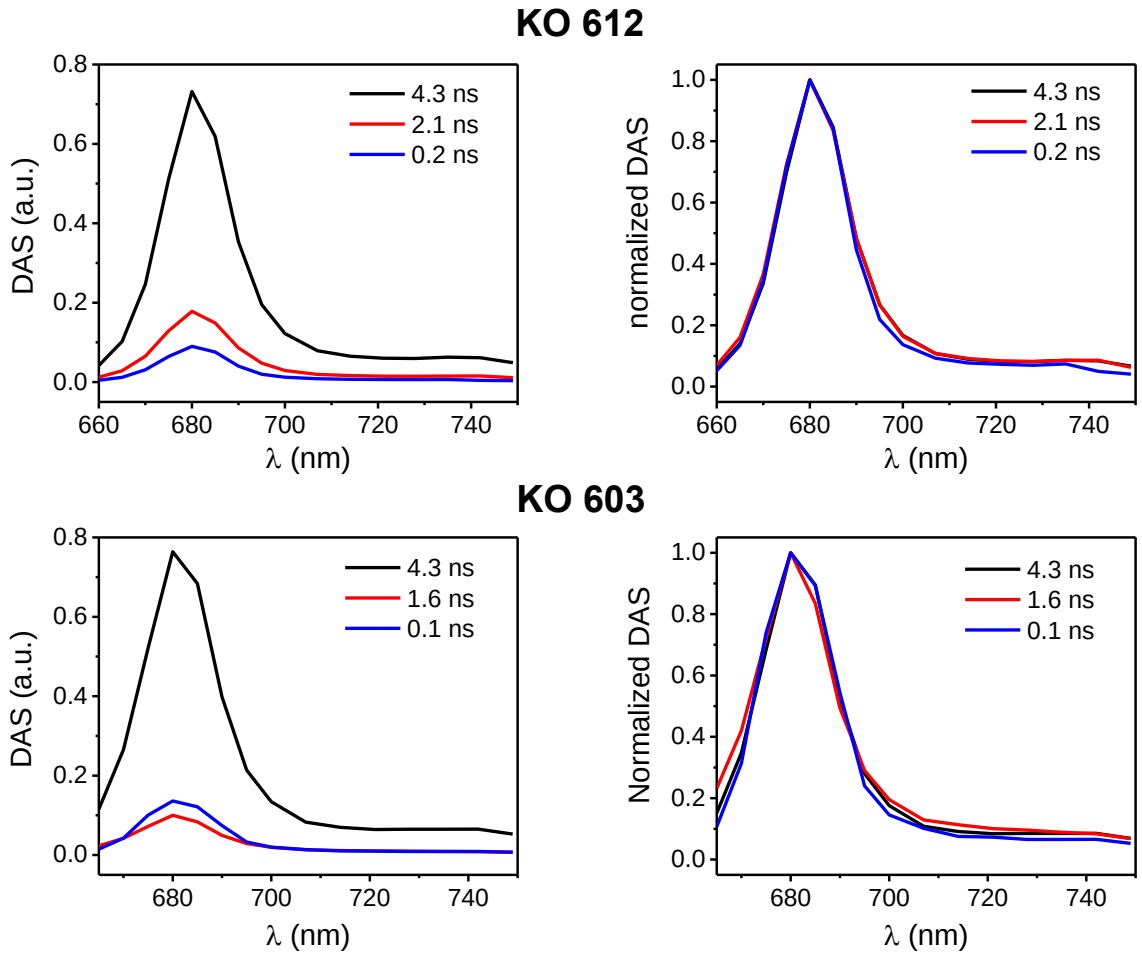

Figure S15. Fluorescence lifetime components of CP29 mutants (related to Figure 2). DAS (left) and normalized DAS (right) for time-resolved emission of CP29 KO612 (top) and KO603 (bottom) upon 468 excitation.

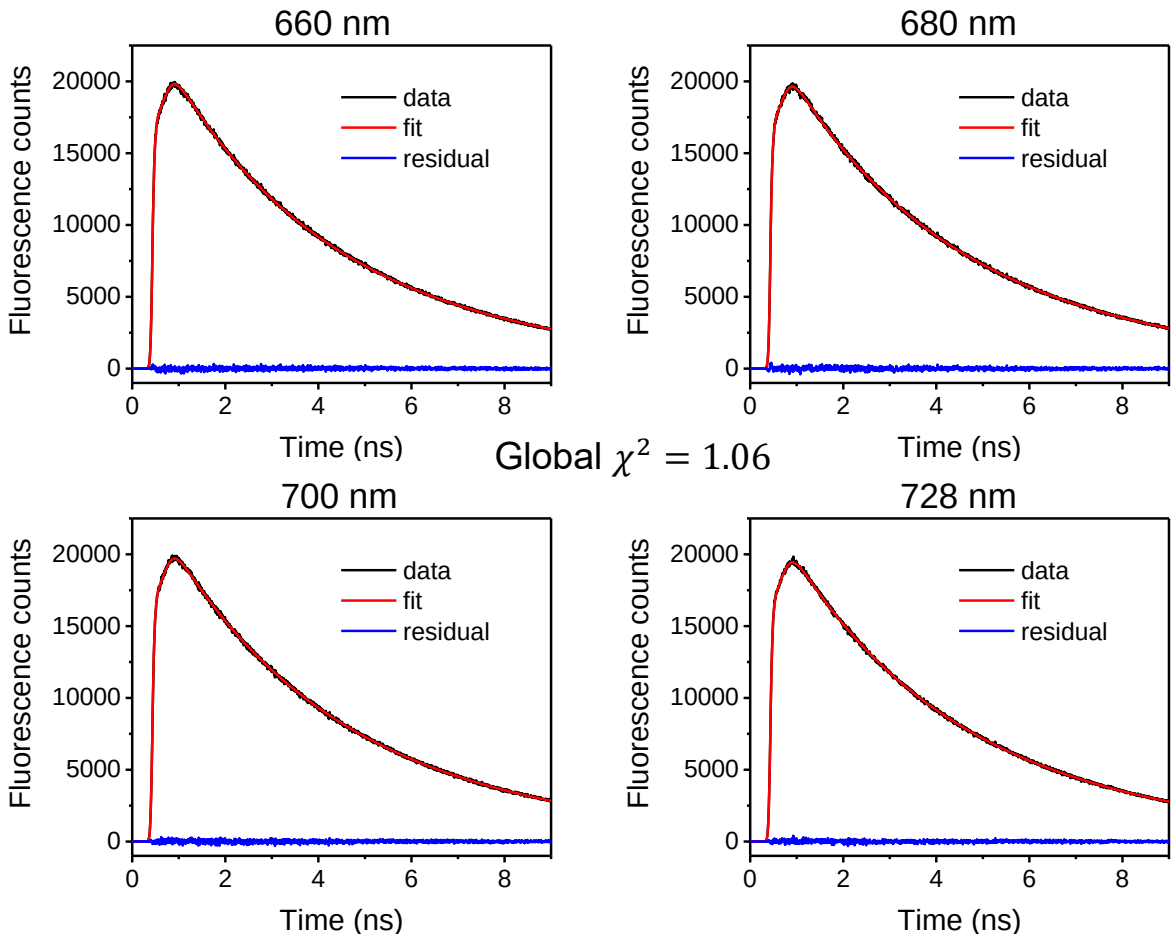

Figure S16. Time-resolved fluorescence experiments on CP29 KO612 at multiple wavelengths. Measured (in black) and fitted (in red) fluorescence time traces at selected wavelengths for CP29 KO612 upon 468 nm excitation. Residuals are displayed in blue.

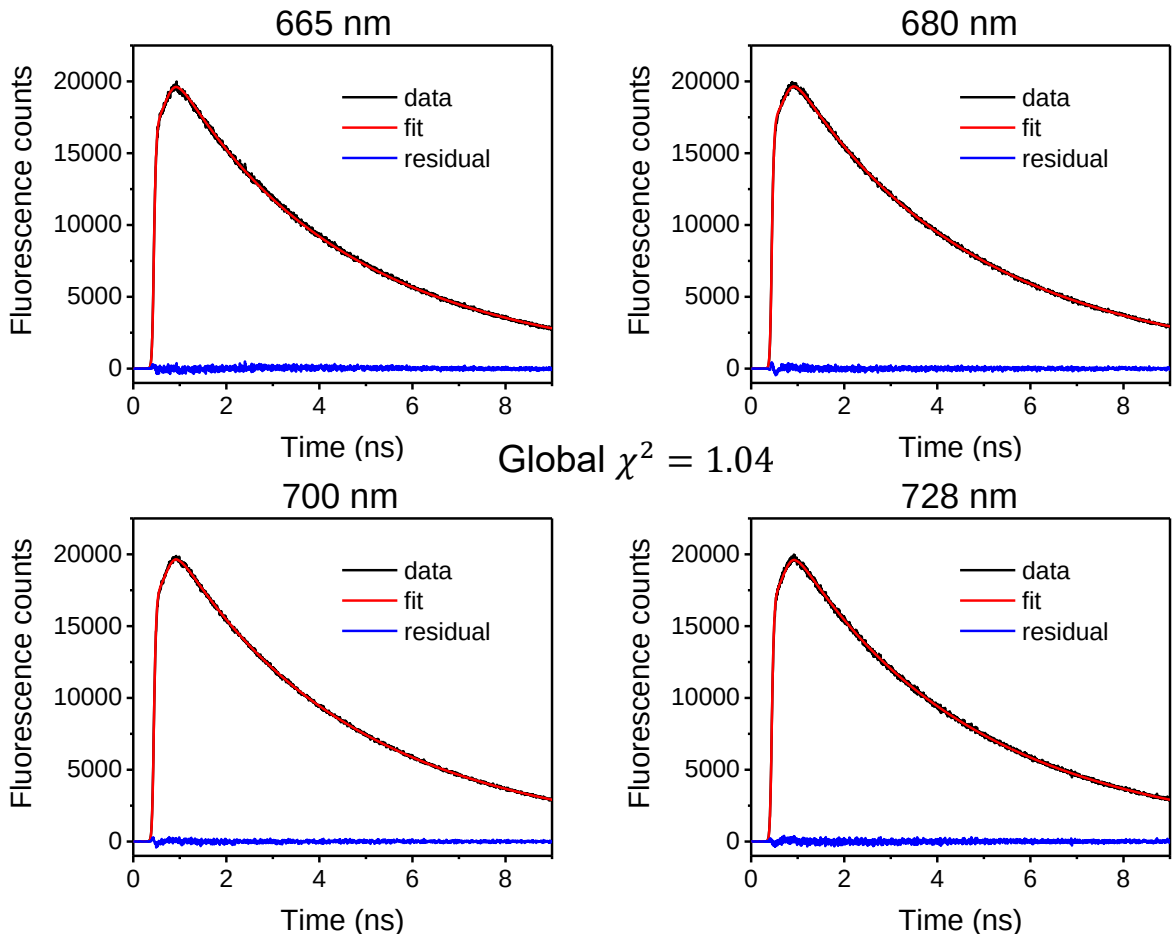

Figure S17. Time-resolved fluorescence experiments on CP29 KO603 at multiple wavelengths. Measured (in black) and fitted (in red) fluorescence time traces at selected wavelengths for CP29 KO603 upon 468 nm excitation. Residuals are displayed in blue.

Table S1. Lifetime components from transient absorption (related to Figure 5). Lifetime and amplitudes of fast and slow components from exponential fit of TA traces at 680 nm upon 672 nm excitation of CP29 WT and mutants (traces in Figure 5 of the manuscript).

	τ_{fast}	%	τ_{slow}	
CP29 WT	60 ps	16	2 ns	84
KO 612	-	-	2 ns	100
KO 603	60 ps	15	2 ns	85

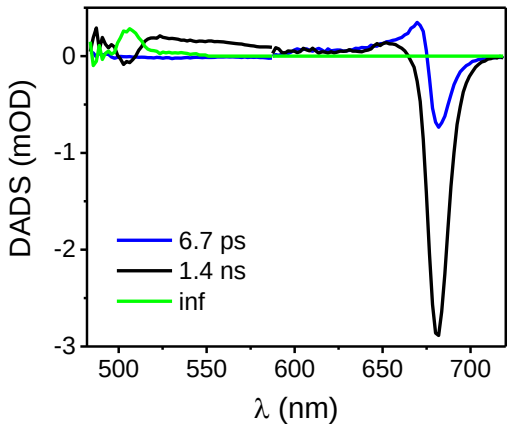

Figure S18. Transient absorption on CP29 KO612. DADS for CP29 KO612 upon 682 nm excitation. Uphill energy equilibration (blue DADS) is followed by chlorophyll excited state decay on a nanosecond timescale (black DADS, whose precise lifetime cannot be determined due to the limited time window of 1.5 ns), which results in triplet formation (green DADS). Due to the very limited fraction of quenched complexes, for CP29 KO612 only the predominant fraction of unquenched complexes is observed in the TA experiments (as can be appreciated in Figure 5 of the main text), whereas no strongly quenched component can be resolved (compare to Figure S5, where an extra DADS with 54 ps lifetime, in red, can be seen for CP29 WT).

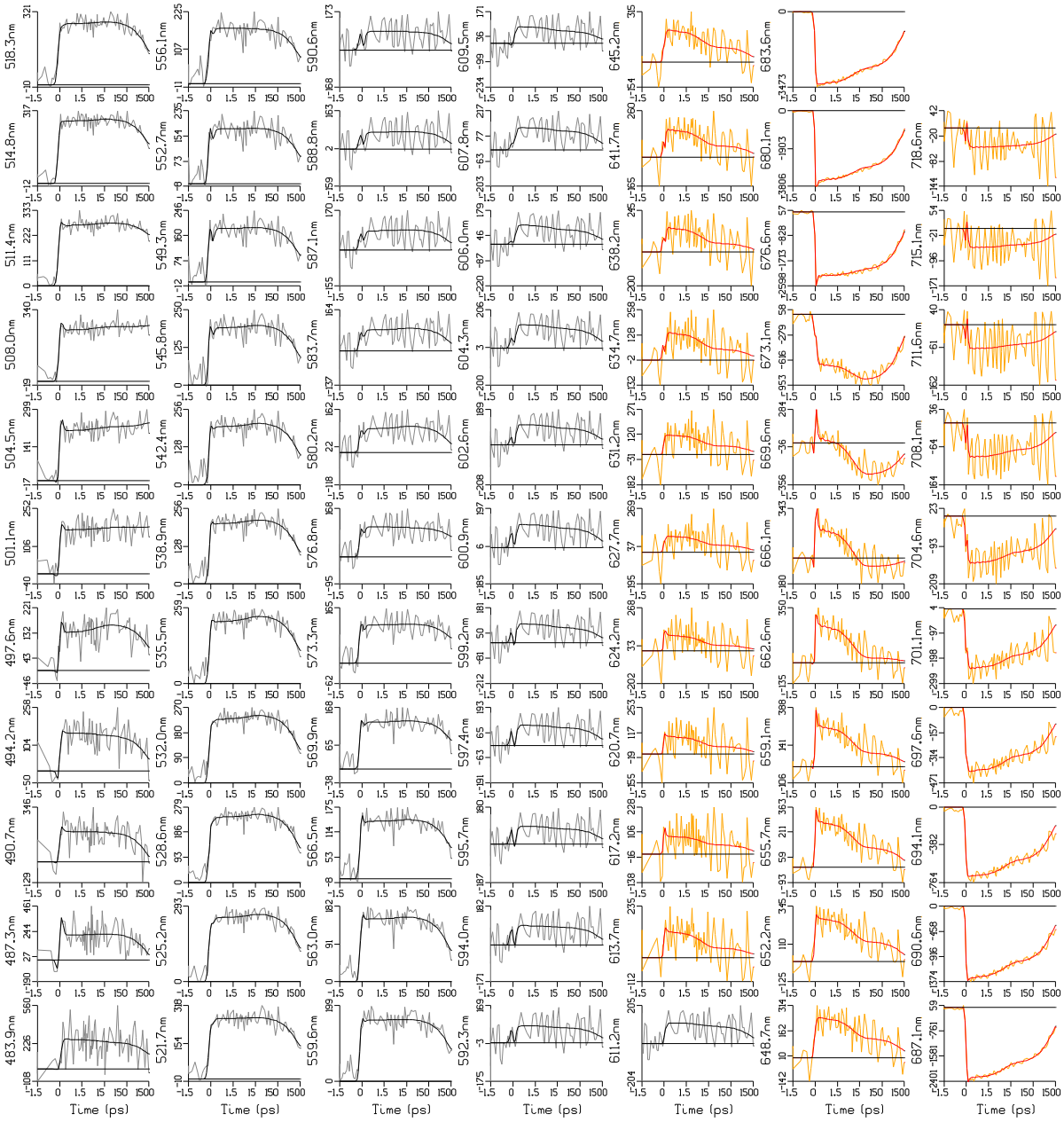

Figure S19. Transient absorption data and fitting for CP29 KO612. Time traces for CP29 KO612 upon 682 nm excitation of raw data (light colors, in µOD) and fit (dark colors) using the kinetic scheme with three DADS (Fig.S18). Wavelength is indicated in the ordinate label of each panel. Please note that the time scale is linear until 1.5 ps and logarithmic thereafter. Please note that each panel is scaled to its maximum.

Text S3. Power study

Transient absorption (TA) traces of CP29 WT measured at 680 nm upon different excitation pulse energies (with 672 nm excitation) and normalized at their minima are shown in Figure S19A. A fast excited state decay caused by annihilation starts to be discernible at excitation energies of 5 nJ per pulse or more. The onset for annihilation was therefore set to 5 nJ/pulse and all relevant measurement were performed below this threshold (3nJ/pulse for 682 nm). For direct carotenoid excitation higher energies could be used (5nJ/pulse at 489 nm and 10 nJ/pulse at 509 nm) due to the much lower absorption at 489 and 509 nm compared to that at 672 or 682 nm (Figure S4). Global analysis on the data matrices recorded at different excitation energies reveal that, above the annihilation threshold, an extra decay component appears, with a lifetime of 10-15 ps, whose amplitude increases with the pump power. Such component can be ascribed to annihilation. On the other hand, the relative amplitude of the 60 ps component, which is observed at all powers, is independent on the excitation energy (Figure S19B). This confirms that the 60 ps component represents a quenching process which is an intrinsic property of the protein ensemble. The lifetime of the power-dependent component is too long to be associated with singlet-singlet annihilation, since the energy equilibration in the complexes is completed on a shorter time scale[42] (around 5 ps). Moreover, the high repetition rate of the pump pulses (40/2 = 20 kHz) suggests that, at increasing powers, chlorophyll triplets can be accumulated on a fraction of the complexes. The interval between two consecutive pulses is indeed 50 µs, much shorter than the lifetime of chlorophyll triplets (on the order of 1 ms[44]), which can therefore accumulate in a significant amount of the monomers since chlorophyll to carotenoid triplet energy transfer is not 100% efficient. We therefore ascribe the observed power-dependent 10-15 ps component to singlet-triplet annihilation, taking place when an excitation is created in those complexes which previously accumulated a chlorophyll triplet. On top of that, singlet-singlet annihilation appears at high powers, resulting in additional signal loss on shorter timescales. The components related to singlet-triplet annihilation and quenched/unquenched complexes also exhibit different spectra in the Qy region, the former being significantly blue-shifted (Figure S19C and S19D). This suggests that the triplet-accumulating chlorophylls are not localized on the terminal emitter domains, consistent with carotenoid triplet quenching being more efficient on the low energy chlorophylls (including chlorophyll 612 and 603, which are also the closest to lutein and violaxanthin).

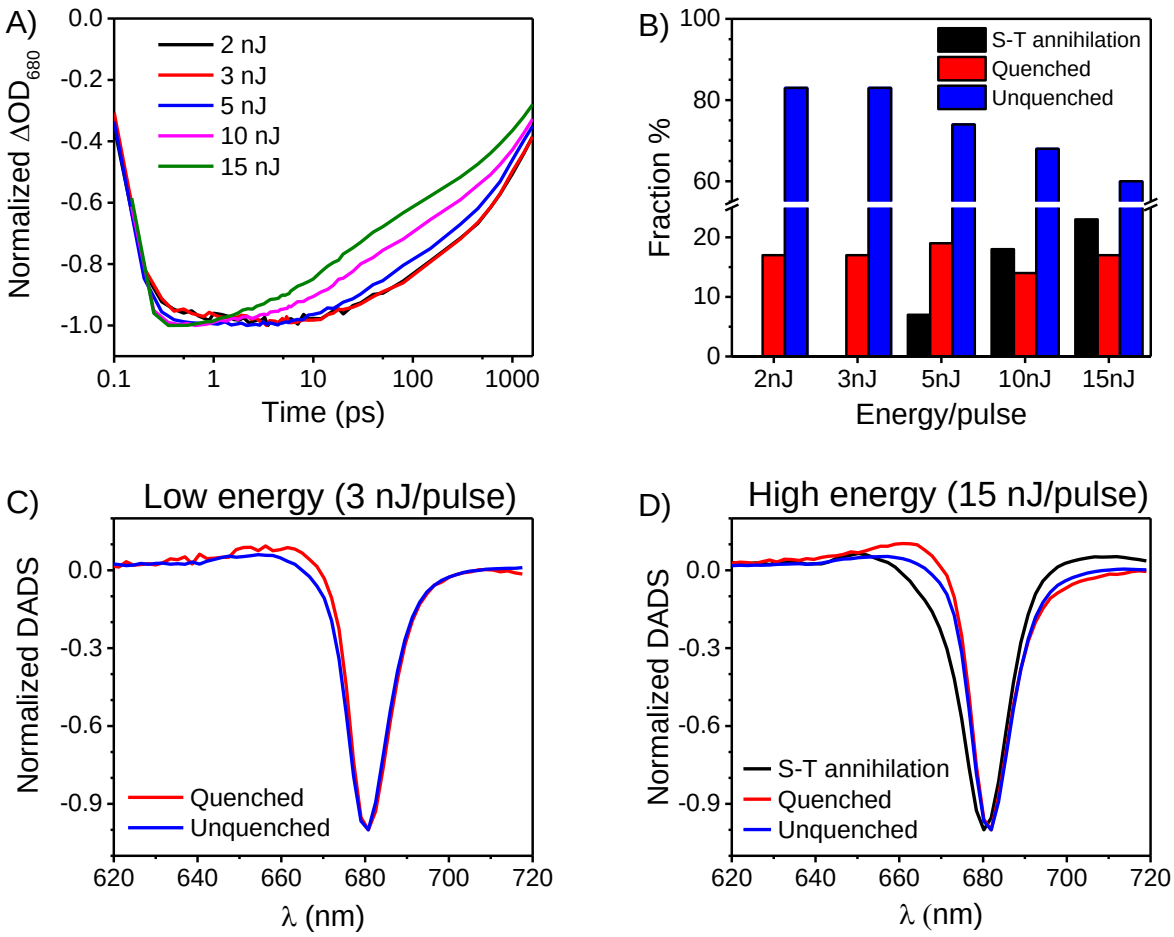

Figure S20. Power study. A) Normalized TA traces at 680 nm measured at different pulse energies (672 nm excitation) for CP29 WT. B) Amplitudes of the decay components obtained by globally analyzing TA data. The black, red and blue bars refer to the 10-15 ps, 60-70 ps and nanosecond components, which are ascribed to annihilation, quenched and unquenched complexes respectively. C,D) Normalized DADS for annihilation, quenched and unquenched components from TA data measured at 3 nJ/pulse (C) and 15 nJ/pulse (D) on CP29 WT.